UNIVERSIDADE DE ÉVORA

ESCOLA DE CIÊNCIAS E TECNOLOGIA

DEPARTAMENTO DE QUÍMICA

Lipid lamellar mesostructures in aqueous media

A study of the influence of temperature and ionic environment on its stacking properties

JOANA RITA RIPADO VALÉRIO

Supervisor: Prof. Doctor EURICO MELO

Master in Chemistry
Specialization Area: *Materials Chemistry*
Dissertation

Évora, 2014

UNIVERSIDADE DE ÉVORA

ESCOLA DE CIÊNCIAS E TECNOLOGIA

DEPARTAMENTO DE QUÍMICA

Lipid lamellar mesostructures in aqueous media

A study of the influence of temperature and ionic environment on its stacking properties

JOANA RITA RIPADO VALÉRIO

Supervisor: Prof. Doctor EURICO MELO

Master in Chemistry
Specialization Area: *Materials Chemistry*
Dissertation

Évora, 2014

UNIVERSIDADE DE ÉVORA

ESCOLA DE CIÊNCIAS E TECNOLOGIA

DEPARTAMENTO DE QUÍMICA

Mesoestruturas lamelares lipídicas em meio aquoso

Estudos de empilhamento em função da temperatura e força iónica.

JOANA RITA RIPADO VALÉRIO

Supervisão: Prof. Doutor EURICO MELO

Mestrado em Química
Área de especialização: *Química de Materiais*
Dissertação

Évora, 2014

Agradecimentos

Porque um trabalho de investigação é impossível de realizar sozinho, várias são as pessoas/instituições que me ajudaram nesta caminhada, ou que me apoiaram fora dela:

Ao ITQB, FCT e DESY por me terem facilitado as infra-estruturas e o equipamento necessário para a realização deste trabalho.

Ao meu Orientador, Professor Eurico Melo, por me ter transmitido o gosto pela ciência e pela descoberta do saber. Foi um enorme privilégio ter trabalho com o Professor, não só pelos conhecimentos científicos que me transmitiu, mas também pela sua forma de estar na vida, que me tornou na pessoa que hoje sou. Obrigada Professor, pela sua inesgotável sabedoria e paciência, sem a sua ajuda este projeto tornar-se-ia praticamente impossível.

Aos professores que me lecionaram as unidades curriculares deste mestrado, em especial à Professora Manuela Carrott, obrigada pela colaboração, disponibilidade e pelos conhecimentos transmitidos.

Á Rita pela companhia, simpatia e dedicação no decorrer destes meses.

Ao Dr. Sérgio Funari pela experiência que me proporcionou, quer a nível científico como pessoal.

To Professor Gruebel for the opportunity to work at the HASYLAB.

Á Catarina e restantes amigos do ITQB pela amizade, conversas e cafés.

Aos amigos e família pela enorme paciência e motivação que sempre me transmitiram.

Aos meus Pais, porque sem eles nada disto era possível e faria sentido. Ensinaram-me a ser Feliz!

Para a minha Irmã, por ser a minha melhor amiga.

Ao Luís, por tudo.

Abstract

Biological membranes are self-associations of amphipathic bilayer-forming lipids in aqueous media, and their physicochemical properties reflect the characteristics of these lipids in interaction with cholesterol, proteins and other components.

In the work here reported we present: *(i)* A study of the thermal expansion of glycerophosphocholines by dynamic light scattering and its consequences for the analysis of X-ray diffraction, and *(ii)* The thermotropism of mixtures of ceramides with fatty acids and discuss the role of fatty acids for the properties of the *stratum corneum* lipid matrix.

We attained in *(i)* A novel interpretation for the lateral thermal expansion of lipid bilayers, how the chain characteristics may affect the expansion, and which are the consequences in bilayer stacking, and in *(ii)* Identify the modifications of molecular mesostructure of ceramide in excess water induced by ionized fatty acid at several ionic strength as a function of temperature.

Resumo

Título: Mesoestruturas lamelares lipídicas em meio aquoso. Estudos de empilhamento em função da temperatura e força iónica.

Membranas biológicas são associações de lípidos em bicamadas em meio aquoso, as suas propriedades físico-químicas refletem as características dos lípidos eles próprios, e da sua interação com colesterol, proteínas e outros componentes.

Neste trabalho apresenta-se: *(i)* O estudo da expansão térmica de glicerofosfocolinas por dispersão dinâmica de luz e as suas consequências analisadas por difração de raios-X, e *(ii)* O termotropismo de misturas de ceramidas com ácidos gordos e a discussão do papel destes nas propriedades da matriz lipídica do *stratum corneum*.

Em *(i)* Apresenta-se uma nova interpretação para a expansão térmica lateral das camadas lipídicas baseada na dinâmica das cadeias, e as suas consequências para o empilhamento de bicamadas *(ii)* Estuda-se as modificações da mesoestrutura de ceramidas em excesso de água induzidas pela adição de ácido gordo em função da força iónica e temperatura.

Abbreviations List

a – cubic lattice parameter
A_l – area per lipid
a.u. – arbitrary units
C10-Cer - N-decanoyl-*sphing*-4-enine
C16-Cer - N-palmitoyl-D-*erythro*-sphingosine
C24-Cer – N-lignoceroyl-D-*erythro*-sphingosine
cac - critical aggregation concentration
CEMOVIS – cryo-electron microscopy of vitreous sections
Cer - Ceramide
Chol - Cholesterol
d – distance between diffraction planes
d_B – bilayer distance
DEPE – 1,2, dielaidoyl-*sn*-glycero-3-phosphatidylethanolamine
DESY - Deutsches Elektronen Synchrotron
DLS – dynamic light scattering
DSC – differential scanning calorimetry
DLPC - 1,2-dilauroyl-*sn*-Glycero-3-Phosphocholine
DMPC - 1,2-dimyristoyl-*sn*-Glycero-3-Phosphocholine
DOPC - 1,2-dioleoyl-*sn*-glycero-3-phosphocholine
d_W – water spacing
e- elementary electronic charge (positive)
FA – fatty acid
FTIR – Fourier transform infrared spectroscopy
FWHM – full width at half-maximum
GUV - giant unilamellar vesicles
H_I - straight hexagonal phase
H_{II} - inverted hexagonal phase
HPLC – high performance liquid chromatography
h k l – Miller indices
I – ionic strength
k_B – Boltzmann´s constant
K_C – bending modulus
LUV - large unilamellar vesicles
L_α – lamellar liquid crystalline phase
L_β – lamellar gel phase
$L_{\beta'}$ – lamellar gel tilted chains
L_c – lamellar crystalline phase
M_I – normal micellar phase
M_{II} – inverted micellar phase
NMR – nuclear magnetic resonance

P – osmotic pressure
PA - palmitic acid
POPC - 1-palmitoyl-2-oleoyl-*sn*-glycero-3-phosphocholine
POPE – 1-palmitoyl-2-oleoyl-*sn*-glycero-3-phosphoethanolamine.
P_{β} - rippled phase
$P_{\beta'}$ - rippled phase tilted chains
p*K*a – logarithm of the acid dissociation constant
Q_I – normal cubic phase
Q_{II} – inverted cubic phase
R – radius of curvature
R_0 – spontaneous radius of curvature.
s - reciprocal stacking distance ($s = 1/d$)
SAXD - small angle X-ray diffraction
SUV- small unilamellar vesicles
T_m – temperature of the main phase transition
T_h – lamellar-nonlamellar transition temperature
T_I – temperature of isotropic conversion to the micellar phase.
WAXD – wide angle X-ray diffraction
γ_l – lysis tension

Table of Contents

List of Figures

List of Tables

I. Introduction

Lipids are important molecules for the backbone of many biological structures. In particular, membrane-forming lipids play the main role in the outer layer of cells and in the compartmentalization of the eukaryotic cells. Their role as barrier components is not confined to cell membranes. The molecules that nature chooses as main components for the protection of organisms from external aggression are also lipids. The external envelope of all mammals is a layer of lipids and dead cells called the *stratum corneum*, SC.

In our work we have dealt with several glycerophospholipids and the physical chemical properties of the bilayers by them formed. We also studied ceramides, a class of sphingolipids that are the key components of the SC lipid matrix.

I.1 The lipids used

The above mentioned lipids are amphiphilic molecules having a polar head group and two hydrocarbon tails that are hydrophobic.

In Figure I.1.1 we show the several classes of lipids that constitute the object of the research presented in this report. The head groups of DMPC, POPC, DLPC and the DOPC are derivatives of phosphatidylglycerol. The choline group is bound to the carbon 3 of glycerol backbone and the carbons 1 and 2 are ester linked to fatty acids. The phosphocholines in Figure I.1.1 show the four main types of chain substitution. In DMPC and DLPC the two hydrocarbon chains are saturated myristoyl and lauroyl acid respectively. Both lipids are symmetric in which concerns chain length and saturation. While in DOPC the two monounsaturated chains are of oleoyl acid. In POPC, carbon 1 is substituted with palmitic acid while in position 2 there is oleic chain. This kind of lipids has been recently denominated hybrid lipids[1]. It is worth mentioning that POPC is the more abundant lipid in animal cell membranes and along the last years a convincement is developed in the scientific community that chemical physical particularities of hybrid lipids are the reason for nature to choose them as the main component of many bilayers membranes.

Ceramides are a sub-class of sphingolipids composed of the amino alcohol D-*erythro* sphingosine esterified to a long chain fatty acid. There are variants hydroxyl substituted but they are not used in the present work. In cells, ceramides are kwon to be involved in several regulation phenomena but, in general, their concentration is very small. Contrasting with this

low abundance in normal tissues, 40% of the lipids constitutive of the uppermost layer of the epidermis of mammals are ceramides[2,3]

It has been shown that they are the key components of the barrier properties of the skin towards water and xenobiotics[2]. In our work we used non-hydroxylated ceramides with different fatty acid chain lengths (C10-Cer and C16-Cer) mixed with different proportions of fatty acids with a variety of chain lengths. The choice of these lipid mixtures is based on composition of the stratum corneum that besides the ceramide contains *ca.* 18% of fatty acids and 40% of cholesterol[3].

Long chain fatty acids are the third most abundant component of the SC lipid matrix. This lipid class is also present in the plasma and other intracellular membranes and is the primary energy source in well oxygenated heart. The physical properties of long chain fatty acids and its phase-behavior in the presence of water are strongly dependent on its ionization sate.

POPC

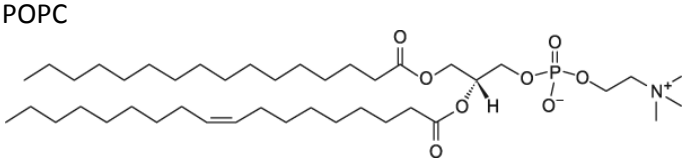

DOPC

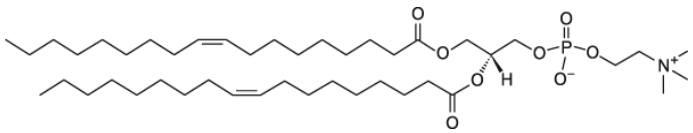

DMPC

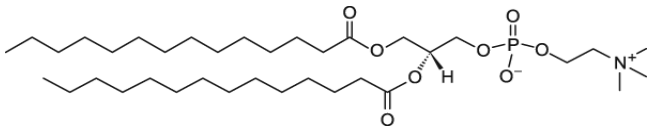

DLPC

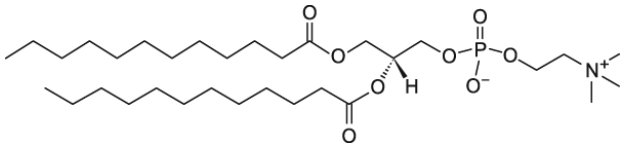

C16-Cer

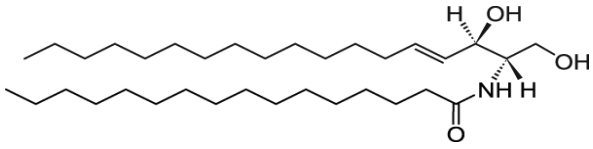

Palmitic Acid

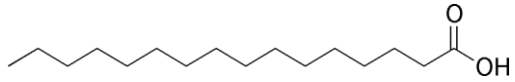

Figure I.1.1. Molecular structure of the lipids studied in this investigation.

I.2. Mesostructures of lipid aggregates

In aqueous solution phospholipids and sphingolipids have a very low critical aggregation concentration, cac, typically lower than picomolar[4,5]. While at first sight counterintuitive, this low solubility is not rooted on unfavorable enthalpic interaction between the hydrocarbons and water, but mainly due to entropic reasons. When dispersed in water the disruption of the water structure and formation of an ice-like nanotube of structured water around the hydrocarbon chain is highly unfavorable from an entropic point of view; an effect know since 1937 as "the hydrophobic effect"[6, 7, 8].

The geometry acquired by the aggregates of amphiphilic molecules is dominated by the geometrical shape of the amphiphile and can be characterized by the critical packing parameter, *P*, defined as [9, 10]:

$$P = \frac{V}{al} \tag{1}$$

where *V* is the molar volume of the acyl chains, *a* the molar cross-section of the polar head groups and the *l* the length of the molecule when extended. The more common structures formed are represented in Figure I.2.1. But many others are possible, namely those where the lipid molecules form cylinders with the polar groups facing outside, the hexagonal H_I, or inside, the inverted hexagonal, H_{II}, of which the H_{II} has been detected in our work. We have also observed several cubic phases where both the lipid and the aqueous phase are bicontinuous, Figure I.2.2.

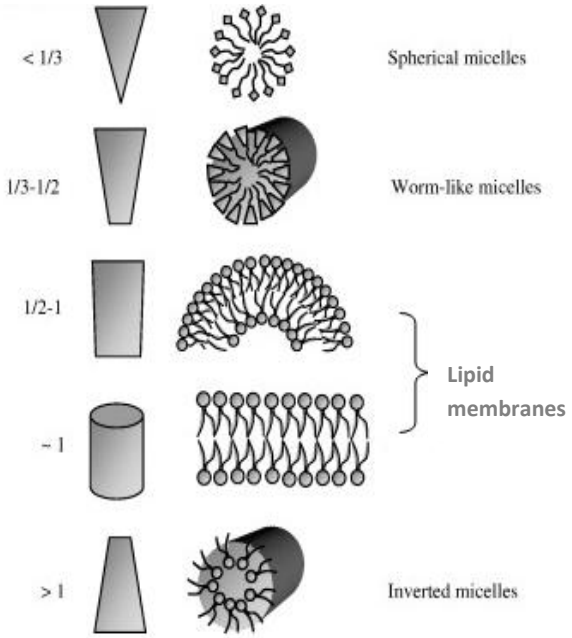

Figure I.2.1. The packing parameter for the most common structures formed[10].

For lipids with packing parameters differing from unity, in excess water, thermotropic transitions frequently take place from lamellar to non-lamellar phases. In this case, above the chain-melting transition, the general sequence for two-chain phospholipids is:

$$L\alpha \overset{T_h}{\rightarrow} \mathrm{Q_{II}} \rightarrow \mathrm{H_{II}} \overset{T_I}{\rightarrow} \mathrm{M_{II}} \qquad (2)$$

where T_h is the lamellar-nonlamellar transition temperature, and T_I is the temperature of isotropic conversion to the inverted micellar phase, MII [11].

The nonlamellar lipid phases are found normally in the fluid state, because this allows greater flexibility in molecular packing. Normal phases are usually found for single lipids with larger headgroups, at high water contents. Inverse phases are usually for two-chain lipids with small headgroups, as it is the case of ceramides, and at low water contents.

The thermodynamics of these transitions is generally determined by the energetic, structural and steric contributions and modulated by non-lamellar structure of the fluid phase[12, 13]. In the fluid lipid phase with radius of curvature *R*, it is possible to determine the tendency of

spontaneous curvature, R_0, and consequently the formation of normal ($R_0 < 0$) or inverted structures($R_0 > 0$)[14].

The hexagonal packing of the water cylinders (H_{II} phases), or lipid cylinders (H_I phases) gives repeat spacings:

$$d_{hk0} = \frac{\sqrt{3}}{2}\frac{a}{\sqrt{h^2+hk+k^2}} \quad (3)$$

In the characteristics ratios 1:1; √3:1; 2:1; √7:1; 3, where the h k is the Miller indices of the two dimensional hexagonal lattice plans[11].
For cubic phases, the X-ray repeat spacings are related to the cubic lattice constant, *a*, by:

$$d_{hkl} = \frac{a}{\sqrt{h^2+k^2+l^2}} \quad (4)$$

Where h k and l are the Miller indices of the planes from which the Bragg reflections arise. Cubic phase either are bicontinuos if both, water and lipid components are continuous, and consist of a hydrated bilayer motif, or are discontinuous in either, the water or lipid components being composed of inverse or normal micelles, respectively[11].

The bicontinuous cubic phases have specific space groups Pn3m, Ia3d, and Im3m, where the minimal surface lies at the midsurface in the water continuum, and consequently the lipid-water interfaces can reasonably be described by networks of interconnected rods. These cubic phases can appear in restricted regions of the phase diagram, and may also be present in excess water.

Cubic phases in excess water, normally, appear between the lamellar and inverted hexagonal phases and may frequently display metastability, as was found for phosphatidylethanolamines[15] and lysophosphatidylcholines[16]. Additionally, Quinn and collaborators[17], explained the formation of a Pn3m cubic phase, by X-ray, in a system with POPE; this cubic phase was stable and coexisted with inverted hexagonal or lamellar phases. This specific cubic phase it was also found in a DEPE system[18].

Inverse cubic phases (Q_{II}) are produced by inverse micelles and, usually, appear following the H_{II} phase as it happens with unsaturated phosphatidylcholines[11].

When dispersed in excess water the glycerophosphocholines form spontaneously closed lamellar phases named vesicles. The formation of closed structures avoids the contact between the hydrophobic region and water, Figure I.2.3. In fact, the structures formed spontaneously are onion-like multilamellar liposomes, MLV, consisting of larger vesicles encapsulating smaller ones with water between the bilayers, Figure I.2.3.

The simplicity of MLV preparation due to their spontaneous formation upon addition of the aqueous media to the lipid "out of the flask" makes them the choice for research and pharmaceutical application whenever possible. When two distinct compartments are needed, separated by a unique stable bilayer or if for some reason the stacking of several layers is inconvenient, other more specific preparation methods are used. However, multilamellar aggregates are the only choice for techniques that rely on the regular piling up of the bilayers such as in the case of small angle X-ray powder diffraction analysis (SAXD).

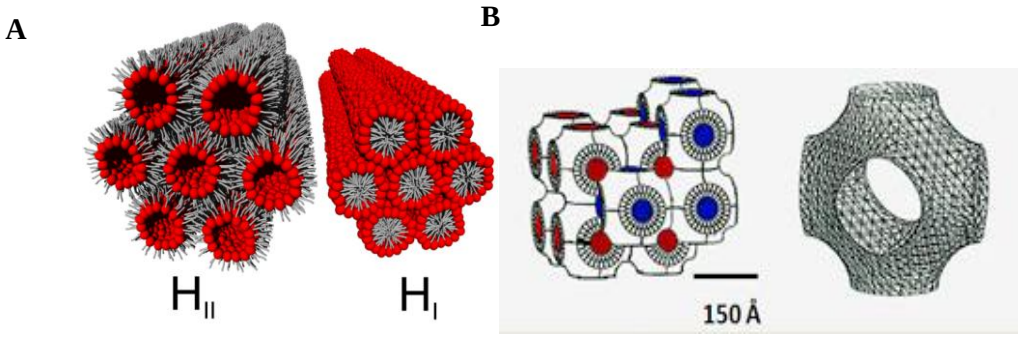

Figure I.2.2. Structures of: A) inverted (H_{II}) and normal (H_I) hexagonal phases. B) Im3m cubic phase. Adapted from ref. [19].

As in general, in bilayers the physical state depends on temperature[20]. At low temperatures the saturated chains are in the all-*trans* configuration rigidly arranged as in a conventional crystal: the lamellar crystalline phase, L_c[19,21]. The crystalline arrangement of the carbon atoms is confirmed by the sharp peaks observed in wide angle X-ray diffraction. At higher temperatures the large rotational and translational freedom of the lipid chains together with a fast *trans-gauche* isomerization lead to a system that can be correctly named as a liquid crystal: the lamellar fluid phase, L_α[19,21]. In some lipids, usually those with a head group cross-section larger than that of the tails ($P > 1$), e.g. saturated phosphocholines, there are intermediate states one of them called rippled phase and the other traditionally named gel

phase, P_β and L_β respectively, or $P_{\beta'}$ and $L_{\beta'}$ if the chains are not perpendicular to the bilayer plane[21]. These different structures are depicted in Figure I.2.4.

The thermotropic behavior above described is valid for pure lipids, in the case of lipid mixtures there are phase separations that are in every aspect similar to what is observed in a binary, ternary, etc. phase diagram for three dimensional systems as they are described in the usual textbooks. The only particularity found is that in the phospholipid lamellar temperature/composition regions were two phases coexist on the plane of the bilayer the phases are micro-disperse[22].

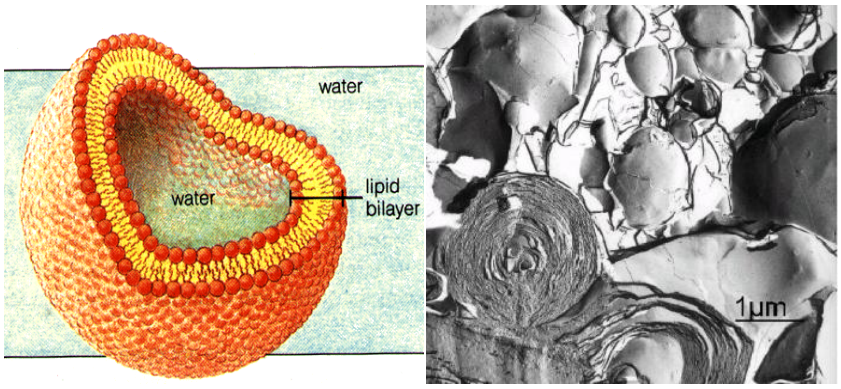

Figure I.2.3. Structures of a unilamellar vesicle and an onion-like multilamellar liposomes.

That means that while in three dimensions the energy of the system is minimized by the reduction of the surface energy, leading to a complete macroscopic separation of the phases, in a bilayer, one phase forms small patches dispersed in a continuum of the other phase, not minimizing the line tension. The reason for this is out of the scope of the present dissertation.

The MLV are useful for several types of measurements namely for X-ray studies, however, its often required to have single layer vesicles that according to their size are denominated giant, (5-300µm), large, (50-500 nm) or small (20nm-50nm), respectively abbreviated as GUV, LUV and SUV [23]. Several methods have been proposed to make each of these types of unilamellar liposomes. In our work we have used MLV, and LUV obtained by extrusion, LUVET. The diameter of LUVET is relatively small of the order of 100 nm [24,25]. In one particular case we needed oligolamellar LUV (with a large central aqueous pool) that were prepared by a variant of the technique known as reverse phase evaporation [26,27].

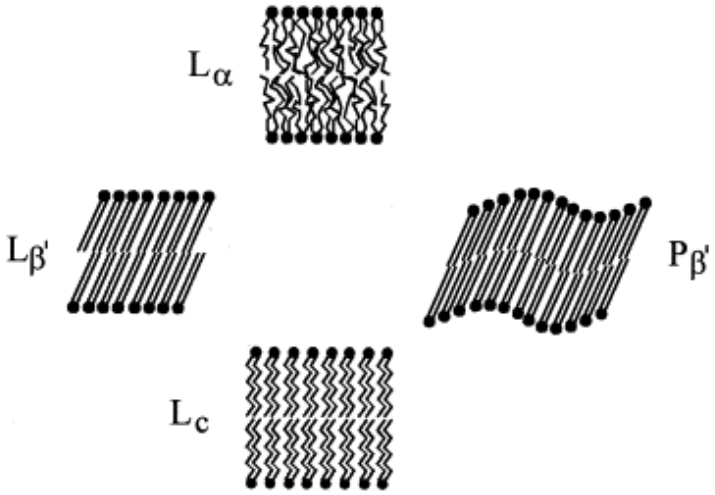

Figure I.2.4. Schematic drawing of lipid–water phases. L_c, lamellar crystalline; $L_{\beta'}$, $P_{\beta'}$, lamellar gel; L_α, lamellar liquid–crystalline (Adapted from ref.[28]).

Ceramides also form lamellar structures but because of being crystalline until very high temperatures and/or because of the very low hydration – thin water layer between *lamellae* – do not form closed liposomes[29].

I.3. Area per lipid

Accurate experimental determination of second-order thermodynamic properties of lipid bilayers against temperature is of high interest for the understanding of their thermophysical properties, since it allows characterizing their thermodynamic behavior, which, evidently, has important consequences from both a fundamental and an applied point of view. They are important elements in the study of model bilayers and their interactions with membrane proteins and other amphipathic molecules, and are an input in computer simulations[30]. Quite extensive discussions about primary parameters such as bilayer thickness and area per lipid molecule, how to define them and which methods are more reliable for their determination, exist since the early days of research on phospholipid bilayers [31, 32]. However, the evolution of properties with temperature, or other physical parameters, was mainly addressed from a mechanistic point of view by E. Evans and his collaborators using micropipette aspiration of GUV[33].

The transversal thermal expansivity of bilayers is straightforward to obtain directly from the analysis of the electron density profiles calculated from SAXD data of stacked bilayers as a function of temperature. Many authors have worked on this subject. The lateral thermal expansivity is another matter since, besides the thickness of the bilayer it must also rely in very accurate measurements of the specific mass of the lipid-water mixture at equilibrium, measurements that are very delicate and difficult to obtain with enough accuracy.

We have recently proposed[34] the use of dynamic light scattering as an expedite method for the determination of lateral thermal expansion and presented a preliminary application to the thermal behavior of DOPC. Our results were in reasonable accordance with those already published for the same lipid; however, the variation of the thermal expansivity with temperature was quite a novelty. We based our molecular interpretation of the data on the recent studies of the isobaric thermal behavior of hydrocarbons. According to the experiments and molecular simulations of Troncoso et al.[35] the isobaric thermal expansivity of hydrocarbons go through a minimum as we observed for DOPC bilayers.

In this investigation, our objective is to make a comparative study of the isobaric thermal expansion properties of bilayers in the L_α phase of pure synthetic lipids, namely DOPC, POPC, DLPC and DMPC. As previously proposed we use DLS for the determination of the area expansion coefficient of lipid bilayers. The measurements are based on the evaluation of the variation of the hydrodynamic radius with temperature of unilamellar vesicles obtained by extrusion, LUVET. For the area calculation the vesicles are supposed spherical.

It was demonstrated that repetitive extrusion of multilamellar lipid vesicles in the L_α phase through filters of 100 nm, or smaller, pore produced a population of homogeneously sized unilamellar vesicles[25,36]. These vesicles are reported to be perfectly spherical if made in pure water and prolate if salt is added due to a difference between the internal and external ion concentration of unclear origin[37]. Being unilamellar, spherical and monodisperse the extrusion LUV are the perfect system for our intended measurements.

I.4. Interactions between lipid bilayers

When lipids are mixed with water form smectic liquid crystals, structures that can be thought as a group of stacked bilayers as can be seen in Figure I.4.1. One of the major goals in studies related with membranes is to understand and describe the interaction between two adjacent membranes, such as the lamellar repeat spacing *d* and more specifically, the water spacing, defined as d_W or d'_W, as well as the bilayers thickness, indicated by subscript B, , represented in Figure I.4.1, satisfying the equation $d = d_B + d_W$[38].

If in equilibrium, the average aqueous spacing between bilayers should be regular and controlled by the interplay between attractive van der Waals forces and the joint effect of several repulsive phenomena. The repulsive forces have several origins: entropically driven steric forces [39,40,41] between headgroups and water frequently called hydration forces, spacing due to thermal undulation, and, for charged bilayers, the double-layer repulsion modeled by the DLVO theory.

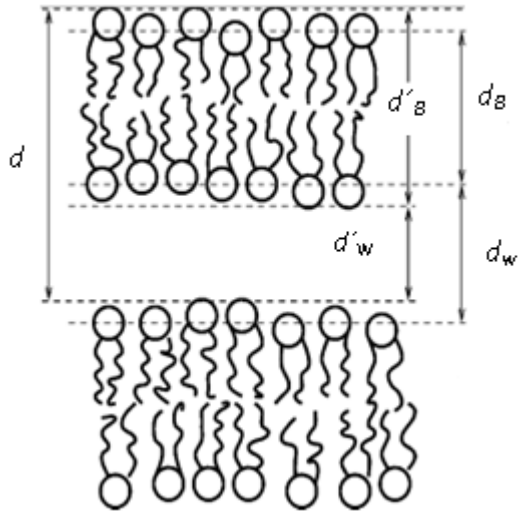

Figure I.4.1. Schematic presentation of two neighboring lipid bilayers (Adapted from ref. [38]).

Local distance variation due to undulations, average all over the system and, in practical terms, is reflected in the SAXD experiments by the extended asymmetric lateral wings of the peaks and is responsible for the difficulty in detecting and characterizing the higher order diffractions [42,43], specially at temperatures above 50 ºC. It is not important for the L_β and L_C due to the membrane rigidity.

Consequently the net pressure between the bilayers is given by[11]:

$$P_R = P_{hyd} + P_{fl} + P_{ES} - |P_{vdW}| \quad (5)$$

Attraction force: The van der Waals contribution is the only long range attractive force, and is what maintains the bilayers together. This force can be quantified by the London-Hamaker constant also called the Hamaker constant, H [44]. The attractive pressure between the bilayer surfaces is given by[11]:

$$P_{vdw} = -\frac{H}{6\pi}\left(\frac{1}{{d_w}^3} - \frac{2}{(d_w+d_B)^3} + \frac{1}{(d_w+2d_B)^3}\right) \quad (6)$$

The Hamaker constant is positive and has been estimated to lie in the range 10^{-14} – 10^{-13} J[11,45] between two planar lipid surfaces. It is worth to notice that while the London potential interaction between two molecules/atoms depends inversely from the 6th power of the distance the dispersion forces between macroscopic surfaces are long-range forces what explains why many bilayer system do not swell indefinitely when water is added.

Hydration repulsion: Even in the absence of undulation, d_W is nonzero what implies the existence of some repulsive force to balance the van der Waals attraction. To this force, whose origin is not totally clear, has been given the name of hydration force P_{hyd}. Rand, Parsegian and co-workers, have proposed a technique that by measuring d and d_W while tuning the osmotic pressure, P allows the quantification of this repulsive force [45].

The hydration force, P_{hyd} may be quantified by an exponentially decaying repulsive pressure of correlation length, λ_{hyd} [45]. These repulsions normally have short ranges, and are supposed to arise from the polarization of the water molecules at the bilayer surface[46]; it dominates for distances in the range d_W = 0.4 – 0.8 nm[47].

$$P_{hyd} = P_{hyd,0} exp\left(\frac{-d_w}{\lambda_{hyd}}\right) \quad (7)$$

Undulation repulsion: When the bilayers are flexible, there is another important repulsive force, called fluctuation force (P_{fl}), where the undulation modes play a role[48].

The fluctuation force arises from thermally excited bending fluctuations of the lipid bilayer, which result in a decrease in entropy when they are suppressed by the approach between two bilayers [48,49]. Helfrich analyzed this force in the absence of van der Waals or hydration interactions, only remaining the steric interactions caused by the collision of bilayers[48]. This repulsive force is important for fluid bilayers at intermediate water spacings from d_W = 0.8-1.0 nm up to the equilibrium separation[47].

$$P_{fl} = P_{fl,0} exp\left(\frac{-d_w}{\lambda_{fl}}\right) \quad (8)$$

Electrostatic repulsion: For charged bilayers in low salt concentration, it has also to be considered the repulsive electrostatic interaction between the two interfaces. These interfaces are separated by a layer of water that contains an amount of ions that depend of the ionic strength and pH of the surrounding aqueous media. However, the concentration of ions, protons and other, near the interface depends on, and modulates the interface potential, Ψ_0. In our experiments we used ceramide mixed with fatty acid at pH = 9.0. At this pH the fatty acid should be 100% ionized since its pK_a is around 5 in bulk water. It is not so in the vicinity of the membrane for two reasons: first, the [H^+] concentration at the interface, $[H^+]_i$, is not identical to that in bulk, $[H^+]_w$, which is stabilized by an adequate buffer; second, because the molecular environment of the carboxylate group at the interface is diverse from bulk water resulting in a pK_a at the interface, pK_a^i, different from the homogeneous aqueous pK_a^w. The correction for the first effect is done, as we describe below, using the theory of the diffuse electro-chemical double layer developed by Gouy, Chapman, Debye and Hückel in the beginning of the XXth century [44]. The determination of pK_a^i is much more challenging and is traditionally approached by considering that the interface is adequately simulated by a 1,4-dioxane:water mixture with dielectric constant of about 40, an approach that is not convincing. Much better is to stick to values of pK_a obtained in the real systems by non-perturbing techniques such as FTIR of NMR. We are fortunate because our exact system was studied by Gomez Fernandez and Vilallain[50]as we detail below.

The fraction of fatty acid ionized at the bilayer surface, that will determine its potential, can be calculated for a known bulk proton concentration, $[H+]_w$, the fraction of fatty acid ionized, with acidic constant K_a^i, is given by:

$$\alpha = \frac{1}{1+[\mathrm{H}^+]_\mathrm{w}\ \phi_0 / K_\mathrm{a}^\mathrm{i}} \tag{9}$$

where, ϕ_0 is the surface enhancement factor, that is related to the potential at the interface, Ψ_0, by:

$$\phi_0 = \exp\left(-\frac{e\,\Psi_0}{k_B T}\right) \tag{10}$$

where *e* is the positive elementary charge and the other constants have their usual meaning. While it may be considered a rough approximation, because the water layer between ceramide bilayers is thin, we will calculate the potential created by the ionized fatty acid, considered at the surface of the membrane, with the Gouy-Chapman formalism[51]:

$$\Psi_0 = \frac{2k_B T}{e} \quad \sinh\left(-\frac{2\pi\, b\, \alpha}{\kappa A_L}\right) \tag{11}$$

where *b* is the Bjerrum length, given by $b = e^2/4\pi\varepsilon_0\varepsilon\, k_B T$, and the reciprocal screening length, κ, by $\kappa = \sqrt{8\pi\, b\,[\mathrm{S}]}$. The value of A_L, the average area per charged lipid, was calculated for the mixture of C16-Cer:Ch:PA 44:38:18 based on the relative proportions and the area occupied by each molecular species. For C16-Cer an area per molecule of 41 Å^2 was calculated from the lattice parameters[52], and 20.2 Å^2 for PA (taken from the discussion of Casilla et al. [53] on fatty acids cross section), resulting in an approximate area per PA molecule of 180 Å^2. The Debye screening length depends from the concentration of the 1:1 electrolyte, [S], and the value of the relative static permittivity, ε, was taken as that of water, ε = 80. All the other parameters have the usual meaning.

Of course the equations (9) to (11) are implicit in α because the interface potential depends on the fraction of ionized fatty acid which, in turn, depends on the product $[\mathrm{H}^+]_\mathrm{w}\phi_0$, the effective proton concentration at the interface, $[\mathrm{H}^+]_\mathrm{i}$. Therefore, an iterative calculation is carried out to obtain α and κ for a set of given conditions, A_L, $[\mathrm{H}^+]_\mathrm{w}$ and [S].

Once the conditions of the interface are known it is possible to calculate the electrostatic repulsive pressure that can be approximated by an exponentially dependent screening[54]:

$$P_\mathrm{ES} = 64\ [\mathrm{s}]\, k_\mathrm{B}\, T \tanh^2 (e\ \Psi_0 / 4k_B T) \exp (-\,k\, d_\mathrm{W}) \tag{12}$$

At low surface potentials, the electrostatic pressure for large bilayer separations may be further approximated by[11]:

$$P_{ES} = \frac{2\sigma_s^2}{\varepsilon\varepsilon_0} exp\,(-kd_W) \tag{13}$$

where σ_s is the surface charge density.

I.5. Structure of ceramides

Over the past few decades, ceramides were mainly studied in the context of the only biological tissue where they were well-known to be structural ingredients: the lipid matrix of the *stratum corneum* (SC), the uppermost layer of the skin of mammals. The SC lipids, ceramides, fatty acids and cholesterol, self-organize in lamellar structures that, since long, have been attributed the remarkable thickness of ca. 13 nm. The details of the molecular organization of these lamellae are still unknown. There are many works dealing with these, or related, lipid mixtures, but most of them use complex lipid blends and focus not on the lipids themselves but on replicating/explaining the properties of the SC[55] However more recent images of the SC obtained by CEMOVIS, Figure I.5.1, show a lamellar repeat distance that seems built from 4.2 nm thick subunits not all of them with the same electron density forming multilamellar stacks, not limited to 13 nm. [56].

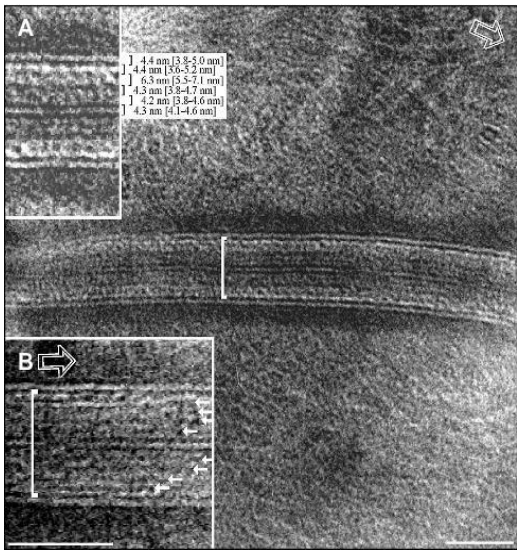

Figure I.5.1. CEMOVIS of the SC lipid matrix [55].

A highly relevant and exhaustive study of synthetic C16-Cer was presented by Shah et al.[57], who examined its thermotropism and structure by DSC, SAXD, and WAXS in the presence and absence of water. Fourier transform infrared (FTIR) has been used for the study of short-range structure and dynamics of C16-Cer in aggregates[58,59,60]. Comparison of the dependence of the chain dynamics and thermotropic properties of C14-Cer, C16-Cer, C18-Cer, and C20-

Cer using FTIR show little dependence on chain length, at least much weaker than that in equivalent cholines[59]. The work of Shah et al. (1995) was complemented more recently by Souza et al. [52,61] and many questions were left open concerning the effect of the addition of fatty acid to the ceramide plus cholesterol mixture.

The pH of the SC changes in the normal to the skin surface from about 7 in the inner layers to 5.6 in the external surface. This pH gradient exists across a region as thin as 10 μm. The FA is at least partially ionized and its carboxyl group necessarily in contact with water. So, the question remains where is the FA located in the structures depicted in the Figure I.5.1.

In many aspects ceramides are quite particular in their mesoscopic arrangements as first demonstrated by the pioneering work of Paschen and Dahlen[62]. These authors showed that, contrarily to the predictions of Langmuir, hydroxylceramides, namely with 18 and 24 carbons, may adopt a splayed conformation in which the two hydrocarbon chains, instead of the parallel arrangement characteristic of the common amphiphilic lipids, diverge in a V shape adopting different angles between the two chains that depend of the temperature or thermal history of the sample, Figure I.5.2. Another particularity of the ceramides is their high transition temperature at which they undergo a transition from a crystalline lamellar phase to a liquid crystal[52,62]. Therefore, ceramides with chains longer than 14 carbons are crystalline in all or nearly all temperature range of the stability of water in the liquid phase at normal pressure. Again, this makes the ceramides unusual among biological membrane-forming lipids that, even in conditions where the crystalline lateral arrangement is thermodynamically stable, remain trapped in a metastable state, either liquid crystalline or the so called "gel state".

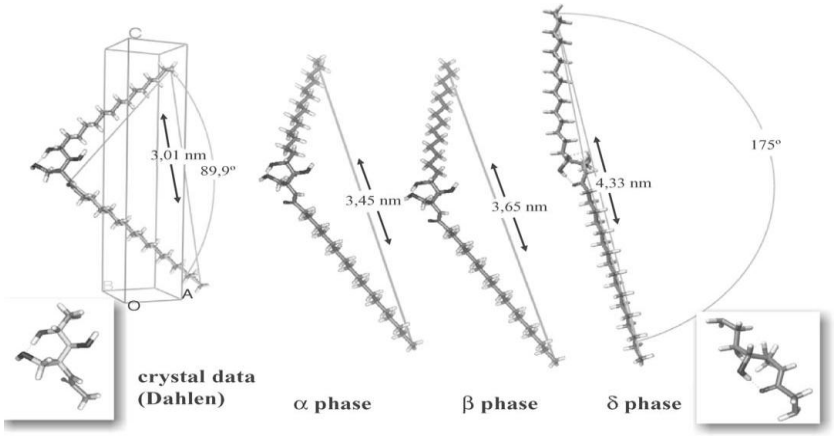

Figure I.5.2. Molecular packing arrangements of hydroxiceramides[62].

Joining the two informations, the splayed structure tendency of ceramides and the CEMOVIS pictures, we raised the question of the characteristics of the mesoscopic arrangement of ceramide:fatty acid mixtures in aqueous media.

Preliminary work obtained by us[63] and by Souza et al.[52], lead to suspect that non-hydroxylated ceramides could also organize in the same splayed conformation of the hydroxylated ceramides. If it was the case, this could explain the detection of what is usually know in the SC literature as "thick phase". This thick phase could result from the disruption at regular intervals of the structure created by the splayed ceramides, Figure I.5.3. These intervals can in certain conditions equal the observed 13 nm obtained by many authors including us.

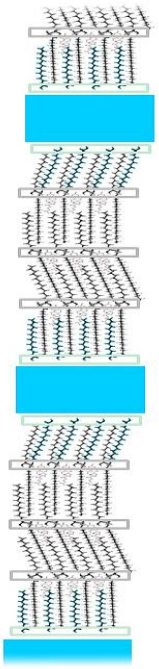

Figure I.5.3. Molecular packing arrangements of hydroxylated ceramides.

One of the major goals of our work was to check the consistence of this hypothesis, with non-hydroxylated ceramides. The reader may question why the use of non-hydroxylated instead of hydroxylated ceramides. This is because in our laboratory we are mainly interested on the properties of non-hydroxylated ceramides with which we have a quite large experience. No doubt that it would be interesting to expand this work to the case of their hydroxylated counterparts.

The thermotropism of pure synthetic ceramide C16 has been already studied[52], it was found that C16-Cer forms a lamellar crystalline phase, that melts at 93 ºC to give a lamellar liquid crystalline phase. On the other hand, mixtures of ceramides with other lipids in the presence of water are the key components of the structure of the lipid matrix of the epidermal layer and are involved in lateral phase separation process occurring in lipid membranes.

To complete our study we also decided investigate the thermotropism of ceramide C16 to which palmitic acid is progressively added as a function of ionic strength using small angle X-ray powder diffraction

When fatty acids are added to ceramide it may be expected that they can substitute one of the ceramide chains without much structural distortion. Our experiments were made at pH = 9,

theoretically allowing complete ionization of the fatty acid (see a detailed analysis in point I.4).
The thermotropic phase behavior of fatty acids is already studied[64] and is influenced by their lyotropism.

When a neutral fatty acid, with a chain length of at least C16, is added to phosphatidylcholines, an inverted hexagonal phase is induced upon system melting, because of an excess of the acyl chain cross section[65,66].

The formation of H_{II} phases, in the presence of fatty acid, is not unusual in mixtures of ceramide[61], phosphocholines and phosphoetilamines at high temperatures [65,67,68].

I.6. Objectives

In this work we will made a comparative study of the thermal area expansion of the lipid bilayers, using the methodology developed by us for measuring by dynamic light scattering the temperature dependence of the hydrodynamic radii of unilamellar monodisperse populations of LUV.

The measurement is based on the evaluation of the variation of the surface area of unilamellar vesicles obtained by extrusion through 100 nm membranes as a function of temperature.

In this investigation, we will report the structural and thermal properties of phospholipid bilayers in the fluid phase, namely those formed by a doubly unsaturated lipid, DOPC, an hybrid lipid, POPC, and two saturated lipids, DMPC and DLPC.

A discussion of the molecular mechanism of thermal expansion and a comparison of the behavior of the different lipids is the main goal of our work.

One of the consequences of the thermal bilayer expansion are the “since ever” observed irregularities in the SAXD measurements as a function of temperature obtained with many lipids that were not understandable until our study. By the time we did this research this abnormal behavior had never been reported in the literature, but was a well-known problem in the lipid community working with X-ray data. We tried to check the several hypotheses raised by different research groups to explain this unexpected misbehavior.

Another work presented in this dissertation refers to the testing of the above mentioned hypothesis of arrangement of ceramides mixed with fatty acid in excess water. As already said, ceramides organize in lamellar structures but do not form closed vesicles. Compared with common membrane-forming lipids, ceramides have the particularity of being in L_c state until temperatures much above physiological. Compared with phosphocholines they have a much less polar head group which results in a much lower hydration. It is not even perfectly clear from what exists in the literature if in excess water the lamellar structures formed involve or not the existence of interlamellar water. A possible conformation has been determined by Pascher and Dahlen[62] involving the two hydrocarbon tails of the single ceramide been separated each one pertaining to a different monolayer. This very rare spayed conformation was proved for hydroxyceramides but never clearly proved if non-hydroxyceramide, e.g. the C16-Cer used in our work, also adopt this arrangement. The first step in this study is to understand the structure of a mixture of C16-Cer and FA at 20ºC.

We have remarked that the mixtures of ceramide C16 and PA have a rich thermotropic polymorphism. Another goal of our study was to characterize the structure of the intermediates in the thermotropic transitions of ceramide: fatty acid mixtures.

Part of this work has already published in ref. 34.

II. Thermal area expansion of phosphocholines bilayers

In this chapter we will present a thermotropic study of the area expansion of unsaturated and saturated phosphocholines: DOPC, POPC, DMPC and DLPC.

These thermal properties were monitored by dynamic light scattering, an expedite method proposed by us for this determination. The measurement is based on the evaluation of the variation of the surface area of unilamellar vesicles, supposed spherical, as a function of temperature.

The consequences of this thermal expansion will also discuss, with the study of structural properties of phospholipid bilayers in the fluid phase, in excess water, by X-ray diffraction.

II.1. Measurement of expansion by DLS

Results and discussion

i) Results from dynamic light scattering

Prepared in the conditions described in the Preparation of Lipid Aggregates section, the LUVET of all four lipids are quite monodisperse in size as it is mandatory for our purpose. Using extrusion, for a given lipid the dimension of the vesicles obtained depend of the conditions of extrusion (applied pressure, flow rate, pore size and temperature) and concentration of the lipid suspension[69,70,71]. Their radius is also dependent of the bilayer physical properties namely bending modulus and lysis tension[69,70,72]. However, we observe small variations in the radius between batches for the same lipid even if an identical filter pore size, 0.1 μm, temperature and applied pressure are used. This is because, in practice, a completely equal manually controlled extrusion pressure-flow rate is not feasible. Due to this variability we made several independent preparations of each lipid until at least 3 identical samples are obtained. Samples are considered identical when at a given temperature their radius is the same within the experimental error inherent to the DLS technique/equipment used: 0.5% in this radius range for measurements made as described in the Methods.

To obtain the external radius of the vesicle the thickness of the adjacent water layer, d_w, had to be subtracted from the hydrodynamic radius. Additionally, since the thickness of the bilayer is not negligible compared to the radius of the LUVET, the area of the bilayer should be defined by a sphere passing by its middle point, the region where the two leaflets juxtapose. Hence, the radius of the vesicle, R_V, used to calculate the area of the bilayer was

determined with the expression $R_V = R_h - d_w - d_l/2$. We consider d_l to be the same for all lipids and equal to 4.6 nm and d_w = 0.24 nm.

In Table II.1.1. we present our results for the hydrodynamic radius at 30 ºC of LUVET obtained as explained above for the phospholipids in study. For the comparison between the several lipids it is useful to recall that, while DOPC, POPC and DLPC were extruded at 25 ºC, DMPC had to be extruded at 30 ºC to ensure being well above its main transition temperature (23.8 ºC) along all the extrusion process.

Table II.1.1. Hydrodynamic radius, R_V, at 30 ºC determined from DLS measurements of the LUVET prepared in this work. We also present values from the literature for the bending modulus, K_c, and for the lysis tension, γ_l, obtained from pipette aspiration, for the bilayers of the same lipids.

Lipid	K_c (10^{-19} J)	γ_l (10^{-3} N/m)	R_V (nm)
DOPC	0.80 [(a)]	10.2 [(c)]	42.1±0.2
POPC	0.85 [(a)]	8.3 [(d)]	43.7±0.2
DMPC	0.69 [(a,b)]	2.7 [(c)]	43.5±0.2
DLPC	0.55 [(b)]		36.4±0.2

(a) from reference [73]; (b) from reference [74];
(c) from reference [75]; (d) from reference [70].

In Figure II.1.1 we show the obtained variation of the radius, R_V, of the LUVET with temperature for the four phospholipids being studied. The temperature ranges between 5-10 and 70 ºC to the exception of DMPC beginning at 27.5 ºC. Below the dew temperature (ca. 17 ºC), and despite the cell holder compartment being dried with silica gel, some of the measurements are entirely out of correlation what we attribute to water vapor condensation on the cell wall and, therefore, were not considered. Instead of the average R_V at each temperature we opted to present all experimental points for the reader to have a better perception of the experimental dispersion. Each of the R_V data points has an estimated error of ±0.2 nm inherent to the DLS measurement done according to the methodology described. However, other particles eventually in suspension, namely micro-bubbles resulting from the decrease of air solubility in water with the increase of temperature, have the consequence of the appearance of spurious experimental values that are clearly identified because the DLS correlation decay curve is abnormal. Those data points were rejected. In Figure II.1.1 the progression of R_V vs. T is qualitatively similar for all bilayers and can be divided in three regions: a region A at low temperature where R_V increases steeply with temperature, a region B where the expansion is much lower, which is followed at higher temperatures by a large increase in R_V, region C. The temperature ranges and thermal behavior of the A, B and C

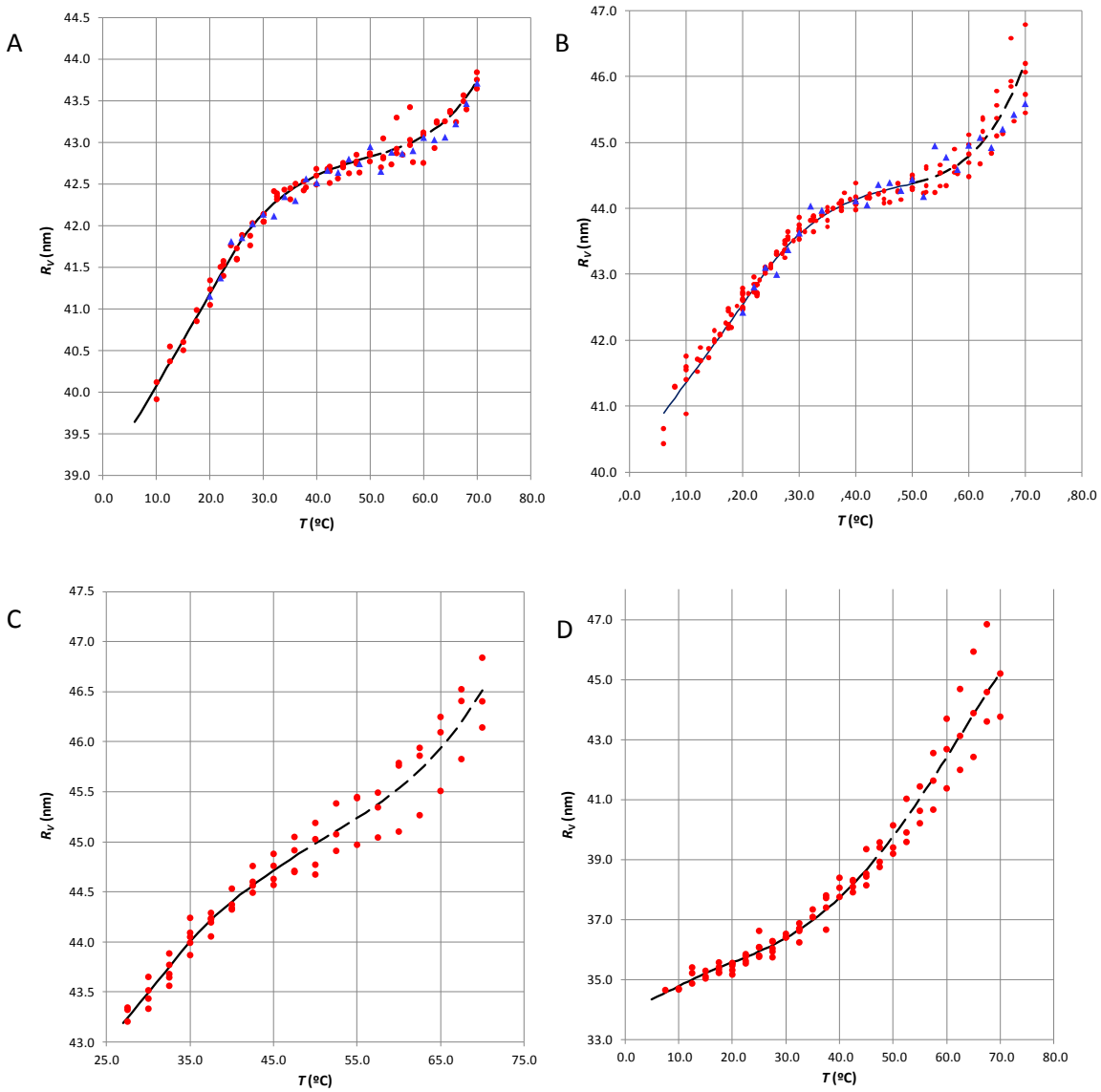

Figure II.1.1. Dependence of the vesicle radius, R_V, calculated from the hydrodynamic radius acquired by DLS of unilamellar liposomes with temperature: A) DOPC B) POPC C) DMPC D) DLPC. The lines are arbitrary functions that have been fitted to the data according to the criteria explained in the text. The triangles in the DOPC and POPC panels were obtained in the cooling of one of the samples and confirm that the LUVET maintain their integrity after the heating runs.

regions is dependent on the bilayer composition. The samples are, at least in which concerns these measurements, quite stable and the radius is reversible with temperature as shown in the Figure II.1.1. panels A and B.

For our final goal, the calculation of the thermal area expansion coefficient, α_A, of the bilayer, a function describing the variation of R_V with T is needed. Since there is no a priori model that can be adjusted to the experimental data we have to rely in the fit of an arbitrary function that describes as well as possible the trend of the data. However, the region A, in particular for the

cases of DOPC, POPC and DMPC is apparently well behaved, meaning by this that the area expansion seems to follow the usual exponential trend observed in common materials when the thermal expansivity is constant. Consequently, the best-fit exponential was used to simulate region A, and the remaining data was fitted by an arbitrary polynomial. The lines in Figure II.1.1 were obtained by this procedure. For DLPC the initial A region is very short and hardly identifiable, probably ending around 15 ºC, but, for the sake of uniformity, we used the same approach in the calculation of the fitted line.

Contrarily to the regions A and B, the region C is not reproducible between samples, and even for a given sample it is extremely disperse. We have denoted this by describing this region with a dashed line indicating that it express the present results but could have another shape if more or other samples were measured.

The area thermal expansion coefficient is calculated with the usual expression, $\alpha_A = (\mathrm{d}A/\mathrm{d}T)/A$, where A is the effective area of the vesicle considered spherical. As said, this sphere is defined by the center of the bilayer, the region of contact between the two leaflets. From the derivative of the above curves we have calculated for each lipid the variation of α_A with temperature, Figure II.1.2. In these curves the sudden change from the constant expansion to the valley corresponding to the region B seems somewhat artificial.

This is the consequence of imposing a "normal" behavior to the region A, however nothing in the data allows postulating a downwards curvature in this region.

The transition between the two regimes, A and B, is certainly not sharp but it is evident and must be stamped in the α_A curves. We think this approach preferable to the alternative of not imposing the usual physical model for region A without being forced to do so by the experimental data.

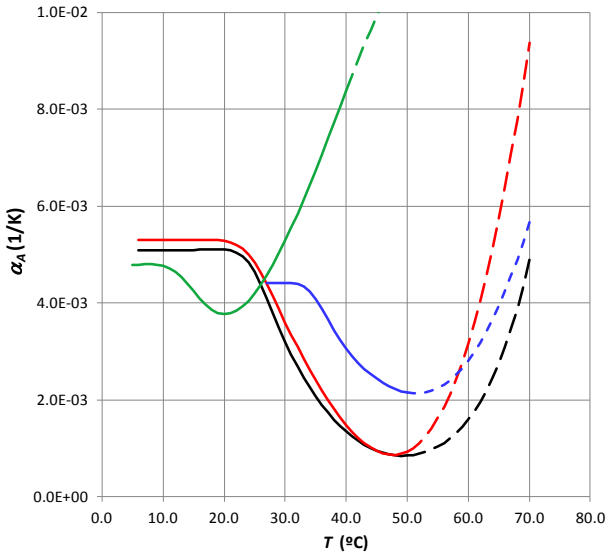

Figure II.1.2. Dependence of thermal area expansivity, α_A of lipid bilayers on the temperature for DOPC (——), POPC (——), DMPC (——) and DLPC (——). The curves are obtained from the variation of the radii of unilamellar liposomes with temperature shown in Figure II.1.1.

ii) DISCUSSION

It is consensual that the size of the LUVET depends on the pressure used for the extrusion, the dimension of the filter pore and, to a certain extent, how many times the extrusion is repeated[76]. In which concerns other conditions such as lipid concentration, flow rate, temperature or characteristics of the lipid, not all works agree. It has been reported that concentration and flow rate do not influence the size of the final vesicles[72]. The lipid composition and temperature determine the physical/mechanical properties of the bilayer, namely its bending modulus, K_C, and lysis (or rupture) tension, γ, reason why it is difficult to accept that the radius of the LUVET are independent of the lipid and extrusion temperature as sometimes said[72]. In our study the lipids were suspended in water and extruded using the same pressure, the same batch of polycarbonate filters and, with the exception of DMPC, at the same temperature. We observed a clear difference between the radii of the vesicles of DOPC, POPC and DLPC, Table II.1.1. This dependence on the lipid, or at least of the lipid properties, has been previously reported. It has been attributed to differences of the bending modulus of the bilayer of the different lipids[69]. The differences in K_C are enough to explain the observed variation in the determined radii of the LUVET, Table II.1.1. The role of the lysis tension is less explored in the literature. It has been said that it determines the pressure threshold for the extrusion[72] and some authors also propose that the vesicle size should increase linearly with

the square root of γ_l[69]. Values of γ_l are not available for all the lipids we would like to compare, and in Table II.1.1 are presented γ_l either derived from the extrusion pressure or pipette aspiration. However, for the lipids under study the trend is not as predicted. As already said the DMPC LUVET radius does not correlate with the bilayer bending modulus retrieved from the literature what can probably be traced to the temperature used for extrusion and goes against the much lower lysis tension reported for this lipid. In any case, in the work of Nayar et al.[36] the egg-PC, essentially constituted by POPC, and DMPC vesicles have the same radius, the first extruded at 21 ºC and the second at 30 ºC.

The pattern of radius variation with temperature is qualitatively the same for all lipids. After a section of uniform increase the variation with temperature becomes less steep but is followed by a second region with large expansion. This variation is pictured in the plots of α_A vs. temperature that exhibit a minimum, Figure II.1.2. Above about 50 ºC the DLS data is quite disperse and due to the uncertainty in the fit curve we represented this region with dashed line. A simple inspection of the heating and cooling data shows that this data dispersion does not result from a disruption of the vesicles because the LUVET maintain their properties unchanged in the time-scale of the experiment.

The in-plane thermal expansion of a fluid bilayer results from three partially independent factors: the usual effect of the anharmonicity of the intermolecular potential energy curve common to all molecular solids and liquids, the increase in the free volume characteristic of liquids, and additionally the progressive increase of the number of the gauche configurations along the hydrocarbon chains. A similar trend is observed for the isobaric thermal expansion of alkanes that was analyzed in detail by Troncoso et al.[35]. The reasoning presented by these authors is based on careful measurements and molecular simulation, and should apply to the case of the lateral thermal expansion of planar bilayers. Their explanation is the following: At low temperature the chains behave like hard spheres similar to other materials but, additionally, there is a component of the expansion that has origin on the trans-gauche isomerization of the hydrocarbon chain both resulting in an increase of the specific volume; the authors do not mention it, but during the low temperature regime certainly a number of voids are already being formed as it happens usually with common liquids. When the temperature attains a certain value that depends of the hydrocarbon in study, the number of voids already present in the system is enough to accommodate the chain conformation changes, reducing the importance of this parcel for the thermal expansion. Similarly, we think that in the region A of the *R* vs. *T* curves the lipid tails follow the normal expansion

mechanism of liquids, probably with the addition of trans-gauche bond rotation also contributing to the expansion. However, above a certain temperature the free volume already present in the bilayer is enough to accommodate increasingly more gauche conformers that are randomly being created along the chains, not contributing, in this way, to the expansion. The hard sphere mechanism is still present and the number of voids increases but, as the amount of free volume is larger, the kinetics of chain rotation contributes less to the expansion. This mechanism dominates the region B. After a minimum, the expansion increases for all lipids, region C. We question if this results from a real increase in the vesicle radius or from the shape of the vesicles diverging too much from a sphere. In this higher temperature region the geometrical shape of the unilamellar vesicles may suffer drastic changes acquiring morphologies that result in a slower diffusion and enhance light dispersion[77,78]. However, the integrity of the vesicles is not affected since, as we show in Figure II.1.1, the process is reversible. A similar increase after the minimum of expansion is observed for long-chain hydrocarbons[35] and alcohols[79]. In the case of the hydrocarbons the invoked reason is the approach of a phase change with the inherent fluctuation in volume and enthalpy. For bilayers the decrease of the hydrophobic effect together with the possibility of interdigitation may result in a particular behavior of the lipids. We know from experiments with fluorescence recovery after photobleaching (FRAP) that the diffusion of a labeled phosphoethanolamine in DOPC, POPC, DMPC and DPPC is abnormally fast above ca. 60-70 ºC probably due to changes of the bilayer structure [W.L.C. Vaz, private communication].

Concerning the region C it is also interesting to observe that for DOPC, POPC and DMPC it begins at ca. 50 ºC and the data is very disperse and sample dependent. The case of DLPC seems quite different from the others in that the decrease of α_A is smaller, the minimum at much lower temperature and the region C begins very early (25-30 ºC). However, like the other lipids, the dispersion of data is only present above 50 ºC indicating that it is the thermal energy and not the expansion regime, A, B or C, that determines the dispersion of *R* measurements.

In region A the lateral thermal expansion goes along with what would be expected from the lipid chain interaction in the sequence: the two unsaturated lipids, DLPC and DMPC. Besides this, DLPC has very short chains and is near the borderline of the membrane forming lipids, the first of which is the dicaproyl PC. According to the model proposed, the temperature at which there is the negative inflection of the *R* vs. *T* curves corresponds to the point where the

free volume created is such that a non-negligible fraction of trans-gauche rotations may take place without space constrains. Therefore we would expect this point to be the related with the chain cohesion, namely with the lipid main transition temperature, T_m. In Figure II.1.3 the plots of Figure II.1.2 are redrawn in a reduced temperature scale, T-T_m. A similar behavior for lipids with identical hydrophobic chain saturation seems to exist, however we cannot make a statement on this due to the small number of lipids tested. There are obvious differences for the minimum of α_A being clear that the existence of double bonds along the carbon chain results in a smaller expansion coefficient probably the consequence of the less organized chain structure.

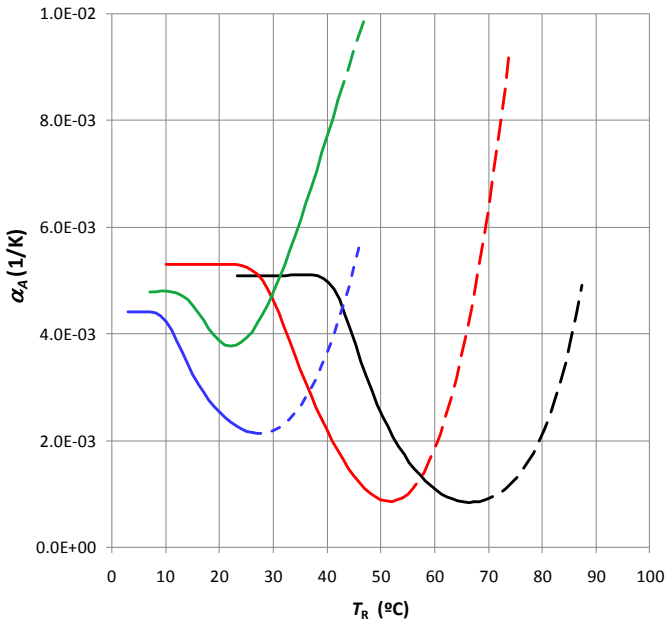

Figure II.1.3. Dependence of thermal area expansivity, α_A of lipid bilayers represented as a function of the reduced temperature $T_R = T - T_m$ for DOPC (——), POPC (——), DMPC (——) and DLPC (——).

Values of α_A are scarce in the literature and those of its variation with temperature, to our knowledge, inexistent. For DMPC at 29 ºC we are aware of two determinations, one from pipette aspiration of giant unilamellar vesicles[80] and another using a variant of the X-ray method of Luzzati and Husson[31] worked out by Costigan et al [81], the first giving $6.8\pm1.0\times10^{-3}$ K^{-1} and the second $3.2\pm0.1\times10^{-3}$ K^{-1}. The values are not far from the 4.4×10^{-3} K^{-1} we have obtained between 27.5 and 35 ºC. However, there are plenty of determinations of A_L, the area per lipid in a reasonably large range of temperatures, for several lipids. The representation of

A_L vs. T will allow not only the estimate of the lateral expansion coefficient as we did for the radius/area of a vesicle with a constant number of lipids but also the comparison with the trend in α_A with T. In Figure II.1.4 we plot A_L vs. T for DOPC and DMPC the source of the data being Costigan et al.[81]. Supposing that the best fit is exponential the lateral expansion coefficients are 3.1×10^{-3} K^{-1} for DMPC and 1.8×10^{-3} K^{-1} for DOPC values that seem to approach our minimum attained at ca. 40 ºC for both lipids in our determinations. Another striking observation is the relative linearity of these plots in a temperature range where ours are obviously curved. What is more perturbing is that their slope is much smaller than that of our linear region. If both results were coincident in the low temperature region and the difference only existed above a certain temperature we could suspect that the curvature in our DLS determination could be an artifact. To this point we do not have an explanation for this disagreement.

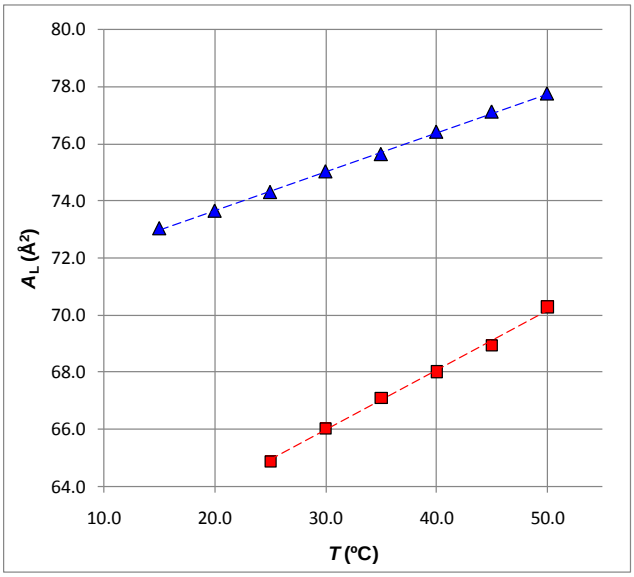

Figure II.1.4. Plot of the values of area per lipid (cross section), AL, as a function of temperature from the data obtained by Costigan et al. [81].The triangles refer to DOPC and the squares DMPC. The dashed lines are linear fits to the data.

It can not be excluded that the values of α_A obtained by us for the region of low temperatures may be influenced by the asymmetry of the LUVET bilayer caused by the excessive curvature of the small radius vesicles that result from an area of the internal leaflet approximately 18% inferior to that of the external one. However there is an aspect that is not taken into account by other authors. Their measurements are not made with equilibrated MLV. As we will explain in Section II.2, due to the slowness of lipid exchange between bilayers only multilamellar vesicles measured at the temperature of hydration are in equilibrium.

II.2. Consequences of bilayer expansion for X-ray measurements

Results and discussion

When there is a change in the temperature of multilamellar vesicles, MLV, the result of the lipid expansion for the stacking of the bilayers is not easy to understand. The surface area of each of the "concentric" vesicles will necessarily increase with temperature due to the bilayer area thermal expansion. In principle the permeation of the bilayer to water takes place within a characteristic time of the order of some milliseconds, or at most a few seconds, making the internal volume freely variable within the time-scale of our observations. Another matter is the amount of lipid material in each layer. Due to their extremely low cac and high activation energy for entrance and exit from the bilayer, long tail phospholipids only exchange between bilayers in a time scale orders of magnitude larger than that of our experiments. This phenomenon should reflect on the stacking of the layers forming an MLV. The work presented here explores its consequences for the small angle X-ray diffraction of MLV when the temperature is changed.

(i) SAXD of MLV and MLV-REV in water. As we expected after the DLS measurements, X-ray diffractograms in the small-angle region of MLV suspensions in water do not always conform to what is expected from regularly stacked systems. Not considering accidental situations where the irregular stacking may be ascribed to a bad sample preparation, it is common to observe a departure from the ideal behavior once the temperature is increased by a few tens of degrees above that at which the system was prepared and/or kept before measurement. In Figure II.2.1 we show the typical thermal evolution of the 1st order SAXD peak of a sample of MLV of DOPC in water made by the technique that we name as film/slow in the Materials and Methods section when heated from 4 to 86 ºC at a 1 ºC/min rate, together with the decomposition in Lorentzians at 4 and 86 ºC. In the diffractogram of Figure II.2.1 panel *a*, the appearance of a shoulder at lower reciprocal distance is noticeable above ca. 40 ºC that eventually develops into a strong peak at higher temperatures. While until 40 ºC a single Lorentzian fits the diffraction peak, having a maximum at $s = 0.158$ nm^{-1} at 4 ºC with full width at half maximum, FWHM, of 0.004 nm^{-1}, at 86 ºC at least three components at $s = 0.142$, 0.150 and 0.174 nm^{-1} are needed to describe the diffraction, panel *b*.

In this and following diffractograms the broadening of the diffraction for high temperatures is to be expected[82], namely the peak should not have a Lorentzian shape. Here we are not concerned with the fit of a theoretical model to the experimental data but with the presence of shoulders and multiple peaks that are not accounted for by the existing models.

An identically prepared sample subjected to freeze-thaw after MLV formation results in a marginally thinner stacking distance at 4 ºC located at 0.159 nm^{-1}. However, increasing the temperature, the behavior does not differ from what was observed with the non freeze-thawed sample except for an improvement in the sharpness of the peaks demonstrating a better spatial correlation. As with the non freeze-thawed sample, to obtain a reasonable description of the SAXD 1st order diffractogram at 86 ºC three Lorentzians are needed, with peaks at s = 0.146, 0.152 and 0.169 nm^{-1}, Table II.2.1.

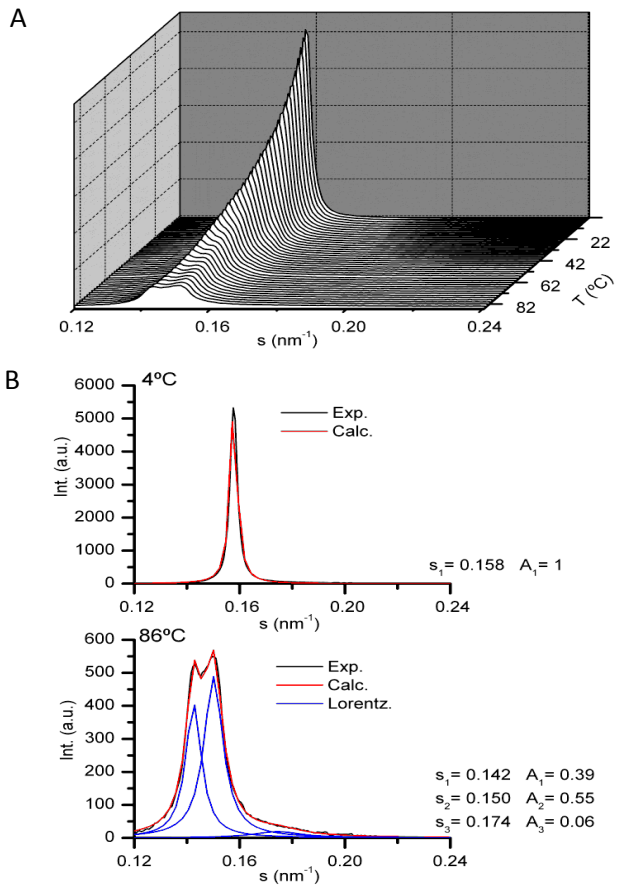

Figure II.2.1. In panel A) the thermal evolution of the sample of DOPC MLV shows the formation of two main peaks, and a shoulder at lower reciprocal distance values, which begin to be visible at ca. 40 ºC. The shoulder eventually originates the long tail described by a Lorentzian at 0.174 nm^{-1} at 86 ºC, panel B). From 4 to 40 ºC the diffraction fits to a single Lorentzian as shown for 4 ºC in B), but increasing the temperature at the rate of 1 ºC/min, at least 2 or 3 components are needed as presented in B) for 86 ºC.

Samples done with fast film hydration, or freeze-dried powder followed by fast or slow hydration, do not result in patterns qualitatively different from the one presented in Figure II.2.1. All samples show non-uniform bilayer assembling above 40 ºC. Fast hydration of the powder presents an apparent better uniformity needing only two Lorentzians at s = 0.142 and 0.153 nm^{-1} to fit the diffractogram at 86 ºC, Table II.2.1, but this is probably due to a poorer stacking revealed by the larger peaks that fit the data, which are twice as wide as those from the other methods, and/or less dense samples, that cause a less favorable signal to noise ratio in the SAXD.

Table II.2.1. Data obtained from the Lorentzian decomposition of SAXD signals at low and high temperature for the lipids tested and several aqueous media and method of preparation characteristics.

Sample	Preparation method	T (ºC)	s (nm^{-1})/normalized integrated intensity from Lorentzian decomposition
DOPC water	MLV film slow hydration	4	0.158/1.00
		86	0.142/0.39 0.150/0.55 0.174/0.06
	MLV film Fast hydration	4	0.158/1.00
		86	0.151/0.50 0.156/0.30 0.158/0.20
	MLV film slow hydration f-t	4	0.159/1.00
		86	0.146/0.49 0.153/0.39 0.169/0.11
	MLV freeze-dry fast hydration	4	0.156/1.00
		86	0.142/0.49 0.153/0.51
	MLV-REV	4	0.152/1.00
		86	0.145/0.14 0.150/0.37 0.205/0.49
	MLV* Constant T	20	0.157/1.00
		40	0.151/1.00
		55	0.149/1.00
		70	0.145/1.00
		85	0.144/1.00
POPC	MLV	4	0.150/1.00

water	Film fast hydration f-t	86	0.135/0.19 0.149/0.55 0.166/0.26
DPPC water	MLV film slow hydration	46	0.146/1.00 (bad fit)
		86	0.144/0.22 0.146/0.24 0.149/0.56

(*) hydrated and measured at the same temperature

The thermal evolution of the reciprocal spacing, *s*, of what we could call the "base component" of the diffraction follows the expected trend with temperature[43,81,83] it slowly increases from 4 to ca. 40 ºC due to the increase in the aqueous layer thickness that is partially compensated by the bilayer thinning caused by chain conformational disorder, and for higher temperatures it systematically decreases due to the increase of the interbilayer repulsive forces. We do not necessarily identify this "base component" with the stronger peak, as will be later discussed. If a common pattern is to be drawn from the generality of the data obtained with the several preparation conditions and a sample heating rate of 1 ºC/min we would say that a single component is present from 4 to ca. 40 ºC, temperature above which one or more shoulders begin to appear at larger and smaller reciprocal distances that for higher temperatures develop in a clear multimodal diffraction. At 86 ºC the strong diffraction consists of the overlap of two components with variable but similar relative intensity separated by ca. 0.01 nm^{-1} accompanied by a third broad smaller band, in several cases prominent, with maximum in the region of 0.16 - 0.17 nm^{-1}. The question may be raised whether this last peak is not a fitting expedient that accounts for the peak asymmetry predicted by the Caillé model[43,84,85,86]. Depending on the sample, this band is more or less pronounced, but even for the "best" samples (freeze-dried fast hydration) its shape is not that of a long tail as the one that can be simulated using the second order approximation of the Caillé's structure factor according to the equations (19), (24) and (28) of Gordeliy et al[43].

The experiments were repeated with other glycerophosphocholines, POPC, and DPPC and in all cases the behavior is similar to that of DOPC, Table II.2.1.

The possible interference of impurities, namely fatty acid and lyso-PC, that can be present due to the time elapsed between preparation and measurement was ruled out by measuring samples of POPC MLV to which lyso-PPC and oleic acid were added simulating 5 and 10 mol% POPC lysis. At 4 ºC the Bragg peak is broader in the presence of the impurities, but a

single diffraction is detected with the maximum shifted by 0.008 and 0.012 nm^{-1} to smaller reciprocal distance, respectively for the 5 and 10 mol% case, probably due to the repulsion of the charged fatty acid headgroups. However, the SAXD multiple peaks that develop at high temperature are neither more pronounced nor differing in relevant aspects from those observed with pure POPC, data not shown, and we conclude that lysis cannot be responsible for the appearance of new peaks.

From these experiments we can conclude that with the increase of temperature at the rate of 1 ºC/min, a non-uniformity of stacking is developed above ca. 40 ºC independent of the method of hydration and diacyl-glycerophosphocholine used. Given that the MLV contain internal "sub-MLV", forming a multi-onion-like structure, where the internal layers have a much higher curvature than the external ones, one possible explanation may reside in a different reaction of the two regions to the temperature. To check for the possible effect of internal smaller MLV we prepared MLV-REV in water that are described as having a multibilayer stacking only adjacent to the external bilayer[26,27]. The SAXD profile, shown in Figure II.2.2, is similar to that obtained with the fast hydration of the freeze-dried sample. However, the lamellar repeat distance is somewhat larger, s = 0.152 nm^{-1}, at 4 ºC the FWHM of the 1st order peak is equally small, 0.004 nm^{-1}, but, despite some non-reproducibility of the method, most samples give good single Lorentzian fits up to 40 ºC. Above this temperature at least two Lorentzians are needed in order to describe the diffractogram: s = 0.145 and 0.150 nm^{-1} together with a very long tail at 86 ºC. Being much noisier than the diffraction pattern of the other MLV used in this work it is risky to affirm that no other peaks are present either at lower or higher s values though they do not appear on visual inspection of the 3D plots. From the experiments with MLV-REV we conclude that the phenomenon observed is not related with the highly curved inner bilayers present in the common MLV. The non-uniform bilayer stacking and the weaker signal of the MLV-REV make the observation less obvious but the effect is present and not qualitatively different from what is seen with conventional MLV.

From the above, two questions are left open: *(i)* are these observations attributable to the difference in the temperature at which the samples were prepared and stored, or are they intrinsic to these bilayers at high temperature? *(ii)* was the heating rate of 1 ºC/min too fast for the equilibration of the system? One experiment that can clarify the first point would be to prepare and maintain the MLV at a stable high temperature beginning with preparation and ending with measurement. Because the procedure is not experimentally straightforward, we

used several samples for each temperature 40, 55, 70 and 85 ºC. In all experiments a sharp and unimodal 1st order peak is systematically obtained, similar to what is observed at 20 ºC with samples prepared at room temperature. Therefore, the complex diffractions have origin in the difference between the preparation and measurement temperatures.

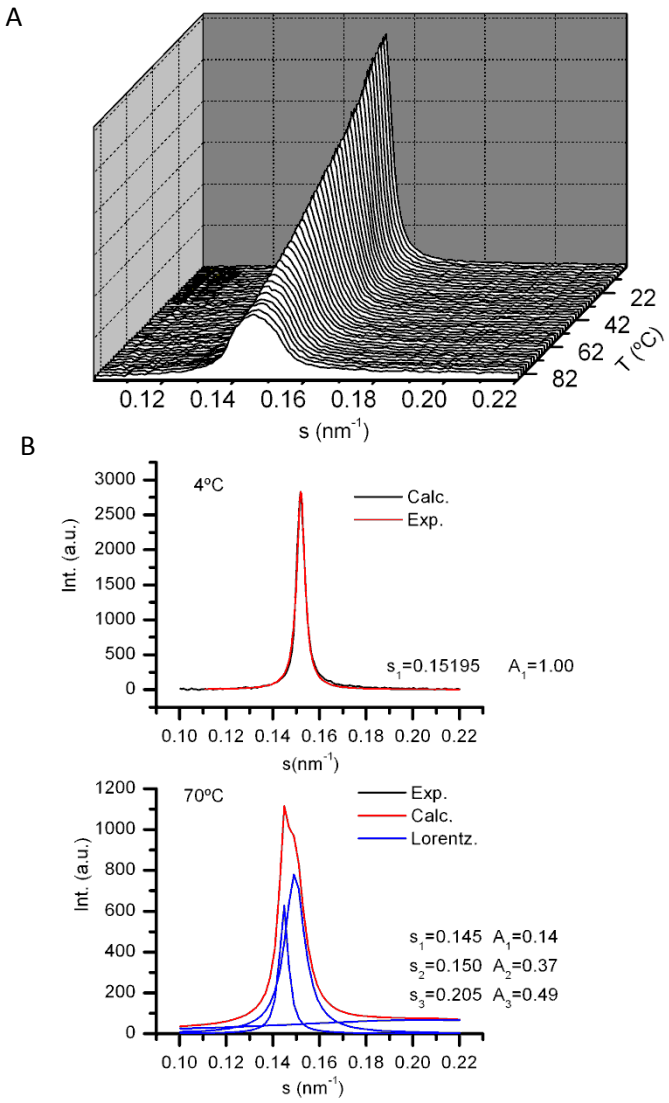

Figure II.2.2. Evolution of the 1st order peak of the SAXD with the temperature, increased at a rate of 1 ºC/min, of a sample of MLV-REV of DOPC in water. In the 3D representation, panel A), no clear shoulders at high temperature are observed similar to those seen in Figure II.2.1, due to the broadness of the peak indicating an inferior spatial correlation. However, above 40 ºC the two Lorentzians corresponding to two visually evident peaks are needed for the fit, as shown for 70 ºC in panel B).

In Figure II.2.3.A), we show the 1st order peak with maximum at s = 0.145 nm^{-1} and FWHM = 0.005 nm^{-1} for 70 ºC, a temperature at which the multimodal diffractions are already conspicuous. The reciprocal distances obtained for all the temperatures studied by this method are presented in the panel b of the same Figure.

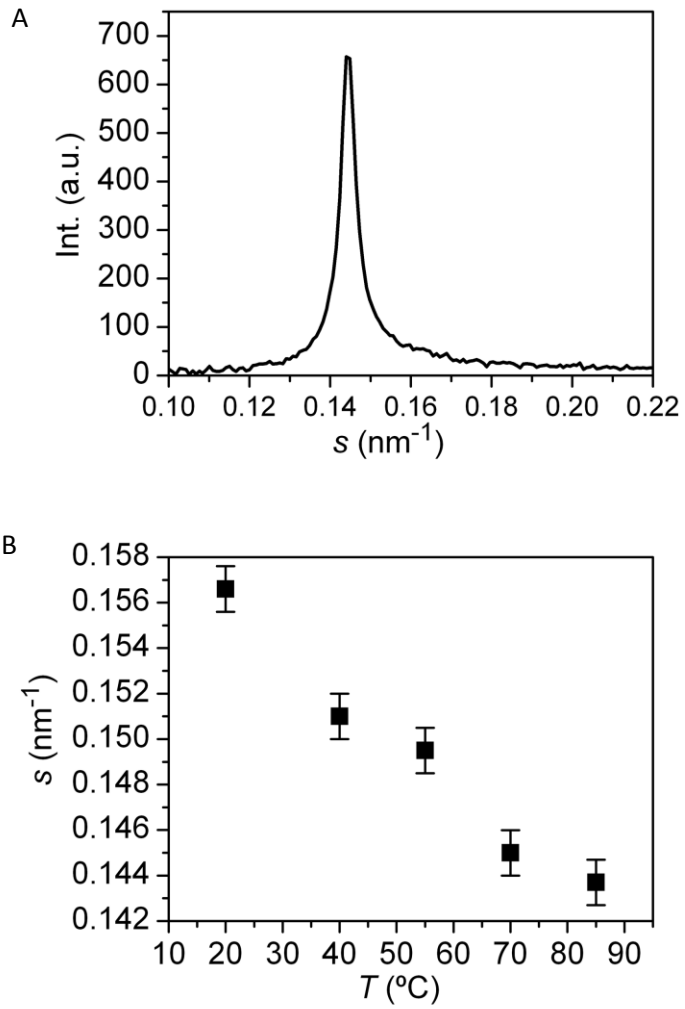

Figure II.2.3. 1st order SAXD peak of samples prepared, maintained and measured at the same temperature as described in the Experimental Methods section. In A) for 70 ºC, the peak is unimodal in contrast to what is observed with those samples prepared and kept at room temperature until measurement. The same happens for 40, 55 and 85 ºC. In B) the reciprocal distances obtained with samples prepared and kept at the measurement temperature are plotted as a function of T.

To find out if the temperature scan rate is too high, samples were heated at a rate of 1 ºC/min from 20 until 70 ºC and then kept and measured every 2 min for 1h at 70 ºC, Figure II.2.4. The sample is prepared by the freeze-dry method with fast hydration at room temperature and the clear shoulder at high s observed in the first diffractograms at 70 ºC disappears in favor of

a sharp 1st order peak at s = 0.149 nm^{-1} with FWHM = 0.005 nm^{-1}, Figure II.2.4. This rearrangement takes ca. 40 min, after which time the peak is unimodal and apparently stable. The behavior is similar for a sample heated from 20 to 40 ºC and left at this temperature for 1 h. In this case the peak is always clean of shoulders but becomes sharper and has a small shift from 0.155 to 0.154 nm^{-1} that also takes about 40 min to complete, data not shown. From these experiments we conclude that the rate of temperature change is the responsible for the appearance of several peaks at high temperature, but it is clear that the spacing attained after one hour at 40 or 70 ºC is not the same that is observed for the sample kept at the same temperature from hydration until measurement, Table II.2.1.

Comparing Figures II.2.3A) and II.2.4, while both, the sample made at 70 ºC and that heated and left to stabilize, have a sharp peak, FWHM = 0.005 nm^{-1}, they differ in their layer spacing by an amount that largely exceeds the experimental uncertainty, the first having a repeat distance of 6.90 nm while that of the sample left to stabilize in the sample-holder only attains 6.71 nm. This difference could result from lysis of the lipid along the 2 days it was maintained at 70 ºC before measurement, but this hypothesis was discarded by TLC analysis of the capillary content. Additionally, the presence of the lysis products should also be reflected in the width of the peaks that is not observed.

The difference in the repeat distance at 70 ºC in these two experiments can only be interpreted as an inability of the sample prepared at room temperature to attain the equilibrium spacing at this temperature. Identical conclusion can be extracted from the 40 ºC experiments.

To summarize, it can be said that until about 40 ºC the behavior of the X-ray diffraction of samples prepared at room temperature is apparently normal, an appearance that is challenged by the observation that the diffraction shifts to lower *s* values if the sample is left at 40 ºC for 1 h. Above 40 ºC the birth of new peaks is observed at lower and higher reciprocal distances, not visible in the perspectives used in the above Figures, peaks that eventually disappear, indicating a complex process in the rearrangement of the several MLV sampled by the X-ray beam. However, if the samples are allowed to stand for time enough at the measuring temperature, a pseudo-equilibrium is attained, that differs from the real equilibrium in having a smaller repetition distance. This process is slow; the time needed for attaining the pseudo-equilibrium for a sample heated from 20 to 70 ºC being close to 2 h what would only be possible with a heating rate much slower than 1 ºC/min.

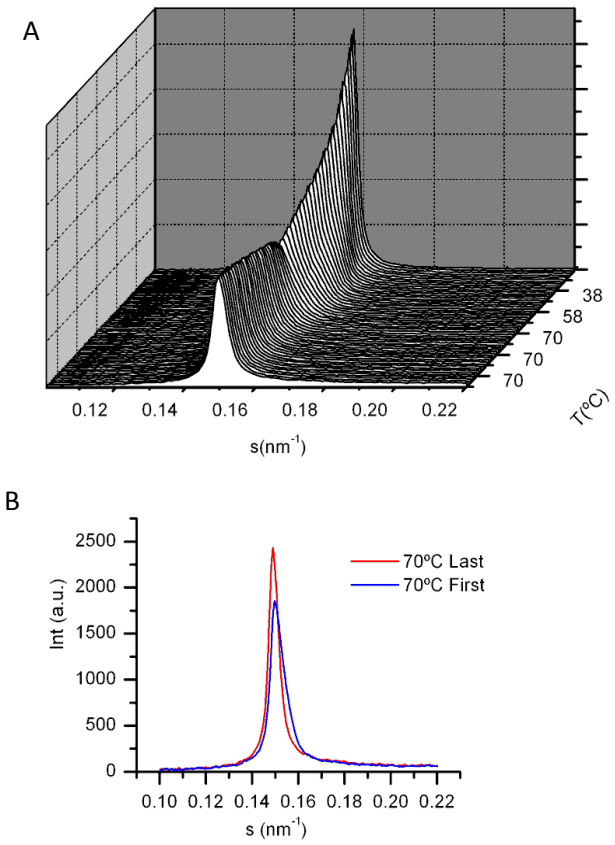

Figure II.2.4. Diffractogram of the sample heated from 20 to 70 ºC and maintained at this temperature for 1 h, panel A. In panel B the first and last measurement of the 1st order peak at 70 ºC.

From what exists in the literature it is not clear why the MLV system has such difficulty in attaining a new equilibrium state. The kinetics of lipid reorganization of MLV in the vicinity of lipid structural transitions after a temperature jump of a few K has been thoroughly investigated[87,88] and the time taken for the system to stabilize is in the sub-10 s range, so it seems that a process with an expected smaller activation energy would be faster to complete. The repeat distance of the MLV bilayers is a function of the bilayer head to head and interbilayer water thickness, both temperature-dependent[81,83], but also of the constraints imposed by the thermal expansion of the concentric vesicles, a trivial geometric effect that, to the best of our knowledge, has never been considered. The thermal area expansion of the bilayer and the reduction of the headgroup to headgroup bilayer thickness are well documented in the literature[81, 89, 90] the same applying to the thermodynamics of the bilayer-bilayer interactions that has been the subject of extensive discussion and theoretical refinement along the past decades [40,43,83 ,85]. However, an aspect that has been neglected is the

geometrical consequence for the topology of the MLV of bilayer thinning and lateral expansion with temperature. In other words – the interbilayer spacing is geometrically forced by the thermal area expansion of the individual layers of a MLV, and the resulting spacing may or not be the one desirable to maintain the bilayer-bilayer interaction at its equilibrium distance. As we will show, to attain equilibrium the lipid should exchange between adjacent bilayers, a process that for long-chain phospholipids is too slow [91,92] to be of practical interest in the lifetime of a sample, not to mention the time-scale of a measurement. The consequence of this thermal area growth for the topology adopted by the bilayers in a MLV is not negligible, as we will discuss in the next paragraphs.

Before trying a detailed explanation of the evolution of the experimentally observed repeat distance with temperature we will concentrate on exploring the consequences of the thermal expansion of the individual vesicles constituting a MLV. The studies of bilayer water permeation are quite consistent in that water crosses the phospholipid bilayer in sub-seconds to seconds[93,94] that is two orders of magnitude faster than the time scale of the X-ray experiments described. It is useful to understand first what would happen to a vesicle with an impermeable membrane when the temperature is changed. When subjected to a temperature increase from an arbitrary T_{ini} until T_{ini} + 50 ºC, the area of the bilayer will expand and, if no water is allowed to cross the membrane, the expansion of the internal water has also to be taken into account. For the present purpose we may consider the coefficient of volumetric thermal expansion, α, of water as constant and equal to that at 30 ºC ($\alpha = 3.8\times10^{-4}$ K^{-1}) in the 50 ºC temperature range of our simulation, and that for the area thermal expansion, σ, of DOPC bilayers also constant and equal to the published value for the same temperature ($\sigma = 2.9\times10^{-3}$ K^{-1})[83,90,95]. Under these conditions, the volume of the water included in a liposome with a radius of 1000 nm heated from T_{ini} until T_{ini} + 50 ºC will grow by 7.9×10^{7} nm^3, but the growth of the area of the lipid bilayer will impose an increase in its internal volume of 9.7×10^{8} nm^3 if the spherical shape is maintained. Therefore, the vesicle must assume a shape compatible with a larger specific surface to fit the small water volume filling its internal space. Any non-spherical shape could satisfy the new geometrical constrains. One possibility is the formation of a prolate spheroid (with axes a = b < c) that, to comply with the relation between volume and surface area will need to adopt an axial ratio c/a = 2.6, geometrically quite far from the original sphere. Generalizing, if the bilayer is impermeable to the water, when the temperature changes from that at which the vesicle was created to a higher temperature, the vesicle will have to change from whatever shape it originally had, in

principle spherical, to a new one with a larger specific surface. What is to be retained from this simulation is the remarkable shape perturbation resulting from the temperature change that may not be 100% recovered in a continuous 1 ºC/min heating of a multilayer system.

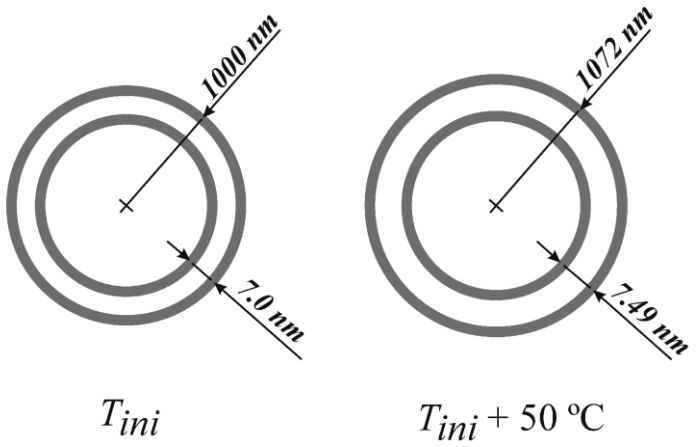

Figure II.2.5. Schematic representation (not drawn to scale) of the effect of the increase of 50 ºC on the geometry of DOPC spherical vesicles considering negligible the exchange of lipid between bilayers freely permeable to water. The initial bilamellar vesicle at a temperature T_{ini} is heated until T_{ini} + 50 ºC supposing the thermal expansion coefficients of the lipid to be constant. The spherical shape and even distance may be maintained, but the interbilayer distance is determined by geometrical factors rather then by the thermodynamic equilibrium distance.

If time enough for equilibrating the inner and outer water is given, no constraints will be created by the independent expansion of the encapsulated water, and only the expansion of the vesicle wall has to be taken into account. To keep the calculation simple we consider only what happens to two concentric spherical vesicles in the L_α phase with a bilayer thickness of 4.6 nm, the external vesicle with radius R = 1000 nm and the internal with R = 993 nm forming a "bilamellar vesicle" as schematically shown in Figure II.2.5. The thickness of the spherical shell separating the two spheres, ΔR, at any given temperature, T, is a function of its separation at the initial temperature T_{ini}, and of the area thermal expansion, σ. If σ is considered constant we obtain the relation $\Delta R_T = \sqrt{1+\sigma(T-T_{ini})}\,\Delta R_{Tini}$. For the thermal area expansion given above, and for an initial separation ΔR_{Tini} = 7.0 nm the thickness of the spherical shell at $T = T_{ini}$ + 50 ºC is ΔR_T = 7.49 nm. In the conditions of this simulation the system will only be at equilibrium if the combined decrease of the bilayer thickness, d_B - d_{Bini}, together with the increase of the width of the aqueous interbilayer region, d_W - d_{Wini} , due to the 50 ºC temperature increase, equals +0.49 nm. This spacing will only by chance be that

interbilayer forces would impose, and to restore the equilibrium phospholipid has to migrate between bilayers, a process that is known to be very slow.

The experiments done at constant temperature from hydration to measurement result in equilibrated samples that allowed the determination of the MLV equilibrium lamellar repeat distance, Figure II.2.3b The distance obtained for 20 and 40 ºC , ΔR = 6.39 and 6.62 nm respectively are compatible with the thermal area expansion calculated in the above section (σ = 4.4×10^{-3} K^{-1}) which is about 30% higher than the literature value for 30 ºC. Therefore, if the published $\sigma = 2.9\times10^{-3}$ K^{-1} is accepted as correct, when heating the MLV suspension the bilayers are not allowed to thermally expand as much as required for the equilibrium distance to be attained, and the system is forced to accommodate at smaller than equilibrium distances. The experimental observation that at higher temperatures several peaks and a long tail develop for larger *s* values (smaller distances) is certainly a consequence of this constriction.

It should be commented that the thermal expansion for DOPC given by Evans and Needham[95], 3×10^{-3} K^{-1}, was proposed more as a guiding number than as an exact experimental parameter, and the more recent determination by Pan et al. [83], giving a virtually identical value at 30 ºC, 2.9×10^{-3} K^{-1}, was obtained for lipids layered on a silicon substrate. In our experiments this value may differ, not only due to the range of temperatures used, but also because the bilayers are not planar.

***(ii) Further comments on the experimental observations*.** For the MLV prepared at room temperature there is no indication of irregularity of stacking until 40 ºC, but this does not mean that the samples heated at 1 ºC/min are at equilibrium. Our purely geometrical calculation based on the thermal expansion of the bilayers would predict a repeat distance smaller than that experimentally obtained. The DLS experiments, while prone to error, confirm that the value $\sigma \cong 4.4\times10^{-3}$ K^{-1} is too large as an average of the area thermal expansion of a DOPC bilayer in the 20 to 40 ºC region, so it seems that the distance is forced to smaller than equilibrium values by the external layers of the MLV. In Figure II.2.6 the evolution with time of the maximum of the 1st order diffraction of a sample heated from 20 to 40 ºC and kept at this temperature along one hour shows that after this relatively long time the repeat distance is still slowly increasing, indicating that the system is not at equilibrium. The change in distance at this slow rate may result from the exchange of DOPC between adjacent bilayers to reduce the compression/expansion to which the inner/outer bilayers are subjected or a readjustment of the several layers to attain a compromise between the possible and the

equilibrium distance and tension. Along this stabilization time it is also evident that the spatial correlation of the layers is improving because, as also shown in Figure II.2.6 the peak is becoming sharper and its maximum increasing.

Above 40 ºC the MLV made and kept at room temperature and heated at 1 ºC/min develop an irregular stacking of the bilayers with shoulders appearing in the diffractograms that eventually give origin to relatively sharp peaks at high temperature. If the heating is stopped and the sample maintained at a constant high temperature these extra diffractions convert in the one at smaller *s* within about 40 min. The system evolves in this time range towards a pseudo-equilibrium state with larger repeat distance that subsequently progress slowly for even larger distance, eventually that found in the equilibrated samples, Figures II.2.4 and II.2.6. What remains to be understood is why, instead of a broad tail spreading to the region of large *s* values, some smaller than equilibrium distances are favored.

The pattern of these multiple reflections is strongly dependent on the method of sample preparation, but whatever the method the final pseudo-equilibrium attained is identical. Since the observed rearrangement is too fast to result from lipid migration, we suppose that the origin of these transient reflections is MLV populations that differ in the behavior to water permeation. In other words, there are MLV that react faster to the temperature, probably because they have fewer and/or more curved bilayers for which water permeation is easier, and others that being bigger and constituted by a larger number of bilayers take more time to adapt to the new geometry.

The observation of a similar pattern with MLV-REV does not invalidate this explanation since the DLS of reverse phase vesicles shows discrete populations of distinct sizes that may originate the same result.

The appearance of non-identical stacking distances only above 40 ºC may be the consequence of the smaller bilayer-bilayer interaction energy at high temperature, that, given enough time, will progress to a shape and distance that is a trade-off between the bilayer-bilayer interaction energy, bending energy, compression and geometrical constraints. Experiments with oriented multilamellar stacks of POPC bilayers deposited on silicon in excess water [96] indicate that between 76 and 80 ºC the repulsive forces overcome the van der Waals attraction originating the so-called unbinding transition.

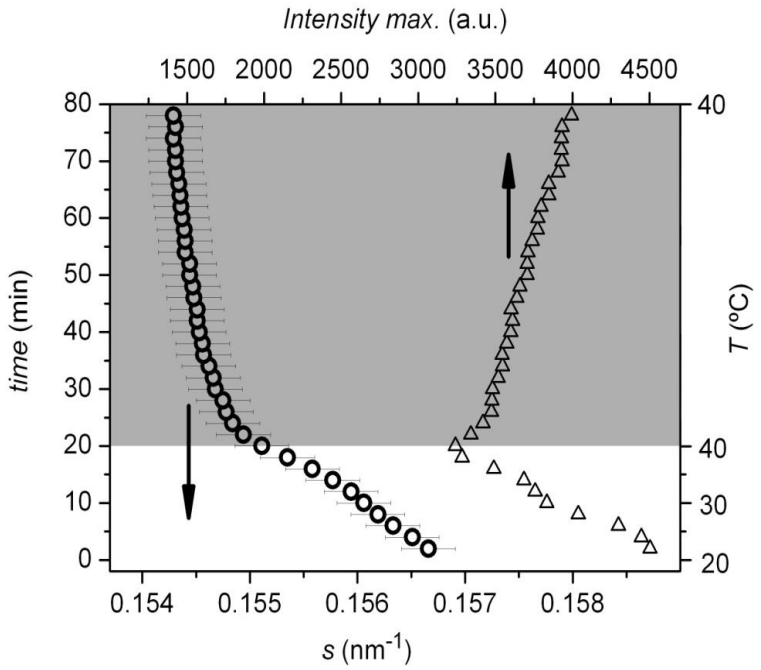

Figure II.2.6. Dependence on time and temperature of the maximum reciprocal distance, *s*, and intensity at peak maximum of the 1st order diffraction of a sample heated from 20 to 40 ºC at a rate of 1 ºC/min and left to stabilize for 60 min at 40 ºC constant temperature (○). Once 40 ºC are attained, there is an initial relatively fast accommodation of the system that takes about 20 min after which the stacking distance continues to increase regularly, without an obvious asymptotic behavior in the time sampled. The intensity at the maximum (Δ) also increases indicating a sharpening of the peak with time. Notice that the *s* scale is unusually expanded.

Following this interpretation, above this temperature no preferred distance should exist between two contiguous bilayers and, even if the multilamellar vesicles maintain its physical integrity, a single broad band should be observed in SAXD, what is not in agreement with the observed results. However, it has also been commented that the observation of the unbinding in that short temperature range may result from the particularities of the preparation, namely the interaction of the bilayer with the silicon substrate[43]. Other authors found that the unbinding transition is not a first order transition, being continuous with onset at 77 ºC for DMPC[43] what seems in better accordance with our observations even if we do not notice a change of behavior at that temperature. It is also worth to note that the same authors conclude that above 40 to 50 ºC, coinciding with the temperature above which the new peaks appear in our experiments, the Helfrich undulation becomes the dominating repulsive force between bilayers. The reduced bilayer-bilayer interactions result in a poorer stacking and in a smaller driving force to attain an optimized shape within the possible boundaries. However we cannot

forget that the encapsulation of the vesicles within each other in a MLV will not allow a separation of the bilayers unless the repulsion is strong enough to break the external layers.

II.3. General Conclusion

In the course of our work we use SAXD-WAXD, a well known technique for the study of lipid systems, and developed a new application of DLS for the study of the properties of unilamellar vesicular structures.

All glycerophospholipids tested, DOPC, POPC, DLPC and DMPC in excess water, present qualitatively similar behavior in which concerns the thermal area expansion. The expansion can be divided in three regions: A at low temperature where R_V increases steeply with temperature, B where the expansion is much lower, followed, at higher temperatures, by a large increase in R_V, region C. We conclude that in the region A the lipid tails follow the normal expansion mechanism of liquids, probably with the addition of trans-gauche bond rotation also contributing to the expansion. In region B the free volume already present in the bilayer is enough to accommodate increasingly more gauche conformers that are randomly being created along the chains, not contributing, in this way, to the expansion. The hard sphere mechanism is still present and the number of voids increases but, as the amount of free volume is larger, the kinetics of chain rotation contributes less to the expansion. After a minimum, the expansion increases for all lipids, region C. In this higher temperature region the geometrical shape of the unilamellar vesicles may suffer drastic changes acquiring morphologies that result in a slower diffusion and enhance light dispersion.

We observed a clear difference between the radii of the vesicles of DOPC, POPC and DLPC which has been attributed to differences of the bending modulus of the bilayer of the different lipids however this trend does not correlate with the role of the lysis tension. DMPC LUVET radius does not correlate with the bilayer bending modulus what can probably be traced to the temperature used for extrusion and goes against the much lower lysis tension.

Regarding the lateral thermal expansion, in region A, follows what would be expected from the lipid chain interaction in the sequence of the two unsaturated lipids, DLPC and DMPC, like for lipids with identical hydrophobic chain saturation. However we concluded a few differences for the minimum of α_A being clear that the existence of double bonds along the

carbon chain results in a smaller expansion coefficient probably the consequence of the less organized chain structure.

The experiments with X-ray diffraction show that the only way to be absolutely sure that the system is in perfect equilibrium is to prepare and maintain the samples at the temperature at which the measurement is intended to be done.

This quite undesirable protocol can be partially circumvented by waiting enough time for equalizing the interbilayer spacing ensuring that a stable single peak is obtained. This "enough time" depends on the measurement temperature and has to be determined for each case. However, we have shown that after this thermal equilibration the sample will not be in its lowest thermodynamic state and the Bragg reflection corresponding to the lamellar repeat distance will slowly shift to larger distances.

All phospholipids tested present the same kind of behavior, which is not a consequence of the particular method of preparation of the MLV samples, or of impurities of the lipid. It is also present when MLV-REV are used showing that it is not related to the particular morphology of the MLV.

The explanation that we propose for this behavior is based on the geometrical constrains imposed by the characteristics of this kind of multilayer assemblies, structures where the migration of lipids between contiguous bilayers is a process too slow to be effective in the time span of most measurement techniques in normal conditions. The consequence is that, besides the force-balance between attraction and repulsion, and the structural thermal oscillations that influence the average equilibrium distance between the membrane interfaces, there are also geometrical limitations created by the thermal expansion of the individual vesicles that force the distance between layers to values that are not necessarily those of minimum free energy.

Due to the identical thermal expansion of all concentric lamellae of the MLV, and in the absence of lipid migration, it is inevitable that the interbilayer spacing eventually differs from the thermodynamic equilibrium interbilayer distance. From the experiments with DOPC it seems that a uniform interbilayer distance is attained in a time that may vary between approximately 30 min and 2 h. It is also clear from the experiments that this uniform distance is not necessarily the equilibrium distance, which for DOPC is significantly larger.

III. Ceramide:fatty acid in excess water

The case of palmitoyl ceramide and palmitic acid

III.1. Cer16:PA at 20ºC in excess water at pH 9 as a function of ionic strength and PA molar fraction

Results and discussion

This chapter will be mainly concerned with one class of lipids, the ceramides (Cer). We discuss the physical-chemical properties and the structures adopted by aggregates formed by ceramides when alone or in mixture with fatty acids along the temperature.

(i) C16-Cer meso and molecular structure in excess water. The visual aspect of the C16-Cer aqueous suspension, whatever the pH, *I* and method of preparation is that of relatively rigid globules floating in the aqueous media. Despite this appearance of wax beads, quite different from a common MLV suspension or a lamellar colloid, the small-angle region of the X-ray diffractograms is clearly that of a lamellar mesophase with a single reflection and the corresponding overtones, Figure III.1.1A). The reciprocal lamellar spacing at 20 ºC, while not changing with pH, is slightly sensitive to *I*, being of 0.223_3, 0.224_1, 0.224_4 and 0.225_8 nm^{-1} (4.478, 4.462, 4.456 and 4.429 nm) respectively for *I* of 76, 125, 200 and 500 mM. The *I* dependence, even if small, is an indication that there is water inside the structure, and that the structure is most probably based on ceramide bilayers. The fact that this dependence is very small may be rooted to the small headgroup dipole moment, as we already discuss, and also result from the H-bonding interactions being more intense between ceramide headgroups than with water.

In Figure III.1.1, panel A), the small angle region of the diffractogram of pure C16-Cer in excess water displays, as we said before, a single strong diffraction at $s = 0.224$ nm^{-1}, during the heating scan, at the same time, an equivalent result has been acquired during the cooling process, results not show.

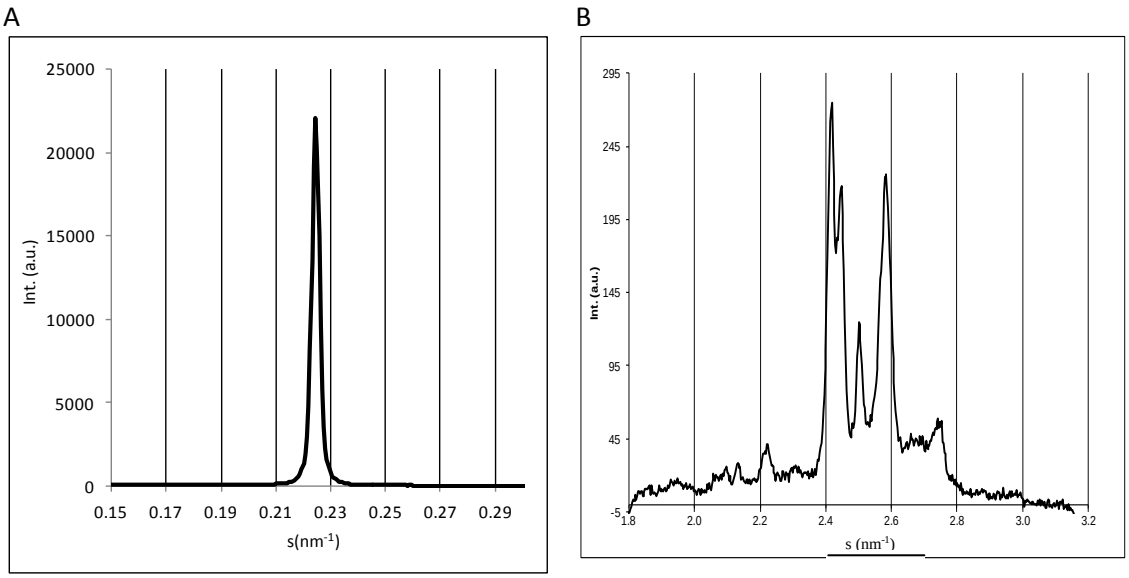

Figure III.1.1. SAXD A) and WAXD B) measurements at 20ºC from pure C16-Cer with 200mM.

At this temperature the wide-angle region is dominated by several intense diffractions, at 2.41, 2.44, 2.50, and 2.57 nm^{-1}, and another much less intense peaks at 2.13, 2.22, 2.74 nm^{-1}. The in-plane structure as measured by WAXD may be reduced to two families of diffraction peaks as presented in Table III.1.1 for 20 ºC that we attribute as pertaining to two phases α and β. Upon heating, the signal of phase α remains quite constant while the peaks attributed to phase β drift to lower reciprocal distances and begin to merge with the remaining peaks at ca. 60 ºC, see a detailed discussion in point III.2 *(iii).*

Table III.1.1. SAXD and WAXD maxima for 200 mM, pH = 9.0 and 20 ºC.

SAXD s (nm^{-1})	0.224_4						
WAXD	Phase α					Phase β	
s (nm^{-1})	2.13_3	2.22_6	2.41_0	2.44_7	2.57_8	2.50_5	2.74_9

(ii) Pure palmitic acid structure. palmitic acid in excess water at pH = 9 and 20 ºC gives a sharp and well defined diffraction in small angle at 0.234 nm^{-1} (4.27 nm) that seems a lamellar structure with a well defined second order at 0.468 nm^{-1}, Figure III.1.2. In the same diffractogram another peak at 0.278nm^{-1} is of unknown origin, eventually also lamellar. Palmitic acid at 20 ºC and pH = 9 forms four strong peaks in wide angle at 2.421, 2.476, 2.606 and 2.774 nm^{-1}, see Figure III.1.2, We did not found a study of the structural prototropism of PA in the literature and the present data is not enough for us to understand what happens with the structure of PA. Anyway, our sole purpose is to be able to verify if there is free PA in our samples.

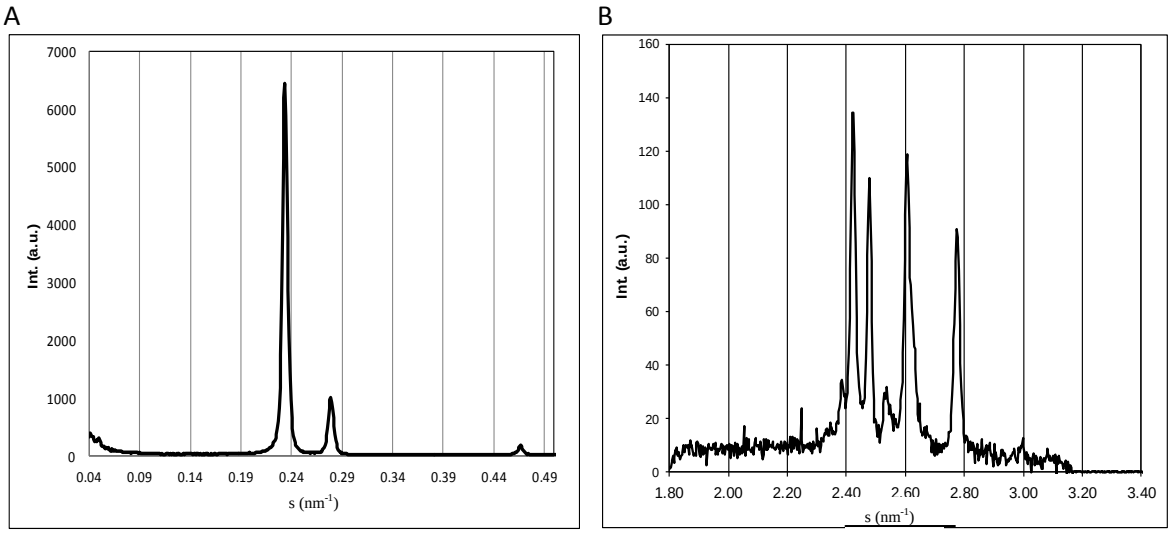

Figure III.1.2. SAXD A) and WAXD B) X-Ray diffraction patterns from pure Palmitic acid at pH = 9 20ºC and with a *I* of 125mM.

At pH = 4.0 it is known that PA forms a lamellar phase with repeat distance is of 3.66 nm and the wide angle reflections are at 2.46 and 2.74 nm^{-1} [61] coinciding with those described in the literature for pH = 5[44], results not show.

(iii) C16-Cer: Palmitic Acid 70:30 structure as a function of *I*. As expected, the mixtures of fatty acid and ceramide show prototropism that is reflected on the mesostructure of the system. The samples at pH = 4.0 in which the fatty acid is in practice fully protonated have the same physical appearance of those of C16-Cer alone and similar SAXD and WAXS (results not show).

The present study refers essentially to the region of complete dissociation, pH = 9.0.The use of pH = 9.0, well above the pK_a^w (PA) = 4.82, ensures that the fraction of non-ionized acid at the membrane interface is negligible. Following a method based on the theory of the diffuse electric double layer previously described, it is possible to calculate the fraction of ionized PA, α, for a specified fraction of PA, pH and ionic concentration.

As previously said the magnitude of the surface-induced shift in the pK_a is not straightforward to calculate and reliable models for its determination do not exist. However, Gomez-Fernandez and Villalain (1995)[50] measured the pK_a of palmitic acid in a ceramide matrix by FTIR at I = 1.0 M and found it to be 6.2. Using the Guy-Chapman model in the backwards calculation and accepting a pK_a for palmitic acid free in water of 4.82 we could calculate that[11] pK_a^i = 5.55. Taking this value, within the limitations of the model, the calculated values of α and interface potential, Ψ_0, for the conditions used in this work are presented in Table III.1.2.

Table III.1.2. Fraction of non-protonated PA headgroups, α, supposed located at the interface of the ceramide bilayers calculated using the method referred in the text for a bulk pH of 9.0 and an area per molecule calculated based on 41 Å^2 for the ceramide [52] and 20 Å^2 for the palmitic acid[61]. The interface potential at the interface plane, Ψ_0, obtained from the same calculation is also presented.

C16-Cer:PA	70:30			
I (mM)	76	125	200	500
α	0.995	0.997	0.998	0.999
Ψ_0 (mV)	-109	-97	-85	-65

In the mixtures of C16-Cer with PA at pH = 9.0 used by us there is no sign of segregated acid until above 70 mol% PA content. The X-ray signals from PA aggregates are easily detected; therefore, at and below 70 mol% PA the acid in the ionized state is included in the C16-Cer matrix, supposedly with the headgroups contacting the interlayer water. These negatively charged groups contribute with a non-negligible electrostatic repulsion between layers that is clearly observed in the larger spacing of the reflections on the SAXD region. At the lowest I used of 76 mM, the I of the buffer salts, the spacing is quite large, in the example displayed in Figure III.1.3A, 17.5 nm, and with the increase of I obtained by a controlled addition of salt, the spacing decreases due to the partial screening of the surface charges as shown in the same Figure panels B, C and D, respectively for 125, 200 and 500 mM. The chain lateral packing in the layers is also modified and the complex WAXS profile for C16-Cer alone converts, with

the addition of 30 mol% PA, into a quite perfect typical hexagonal packing with a single WAXS peak at 2.484 nm^{-1}, Figure III.1.4. Within the accuracy of our measurements this single peak does not move with the *I*, indicating that the lateral packing is not affected by the screening of the charges of the PA headgroups dispersed in the bilayer. The conversion of the original structure into a more symmetrical one may be the consequence of the lateral expansion of the bilayer due to the PA headgroup repulsion increasing the rotational freedom of the hydrocarbon chains, a freedom that does not need to be extended to the ceramide headgroups.

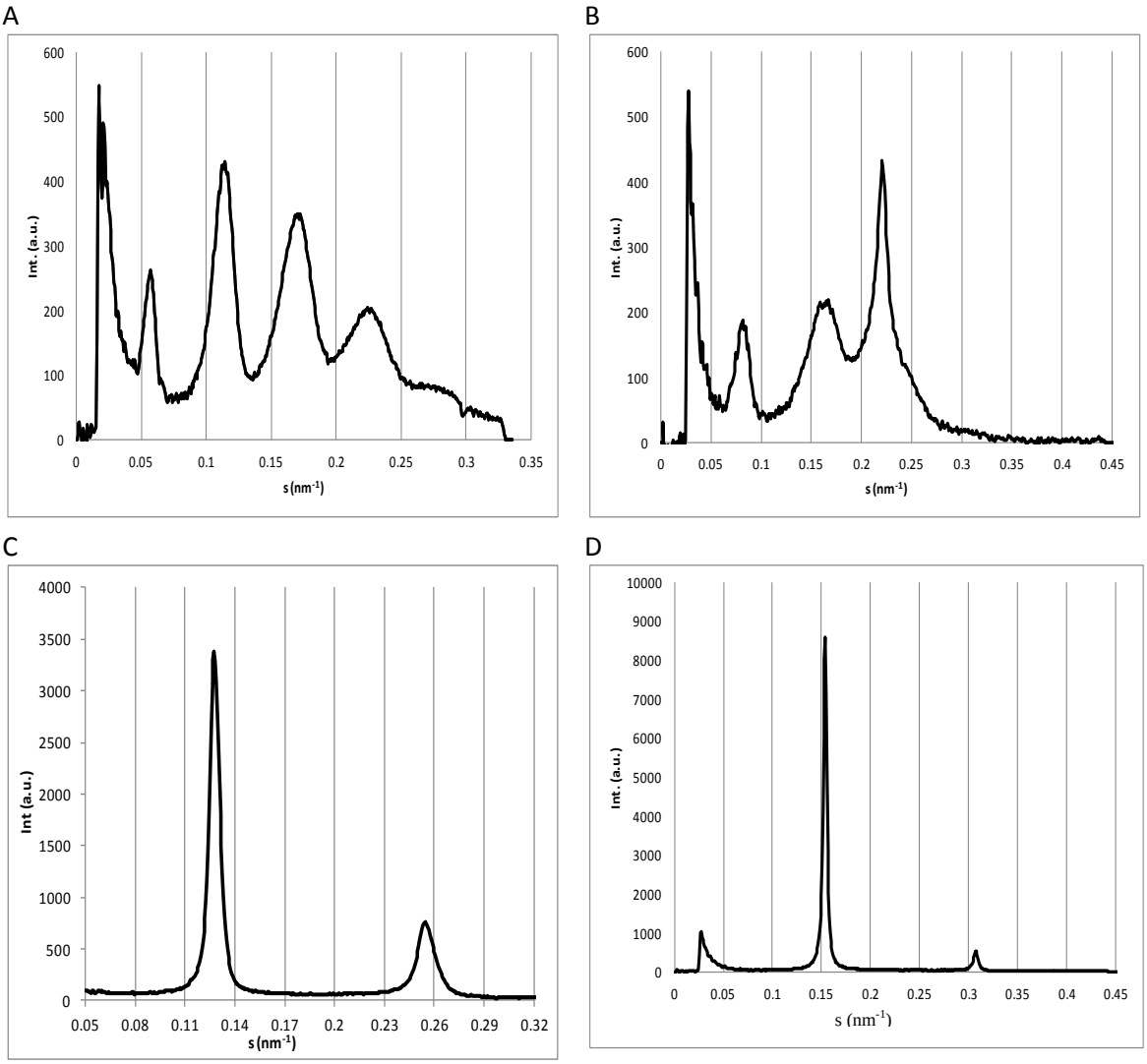

Figure III.1.3. SAXD signals of the C16-Cer:PA 70:30 bilayers at 20 ºC for the *I* of the aqueous medium tested in this work: A)76 mM, B) 125 mM, C) 200 mM and D)500 mM.

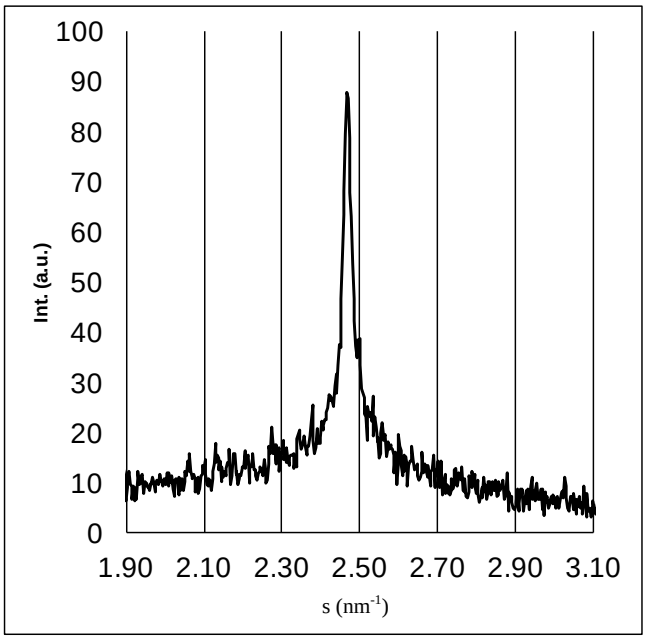

Figure III.1.4. A typical WAXD signal of the C16-Cer:PA 70:30 bilayers at 20 ºC. The represented WAXD is for a sample with *I* = 125 mM, but identical diffractograms are obtained for the other *I* values tested.

The lamellar spacing plotted as a function of *I* in Figure III.1.5 shows clearly that the spacing tends asymptotically to the value of the thickness of pure C16-Cer, represented by the dashed line, with increasing *I*. This leads to the conclusion that we are dealing with single bilayers whatever the *I* and the larger spacing is a consequence of the interbilayer electrostatic repulsion. It also justifies the relatively broad peaks obtained at low *I* values, a broadness that results from the strong undulations allowed by the lousy attractive interactions between layers.

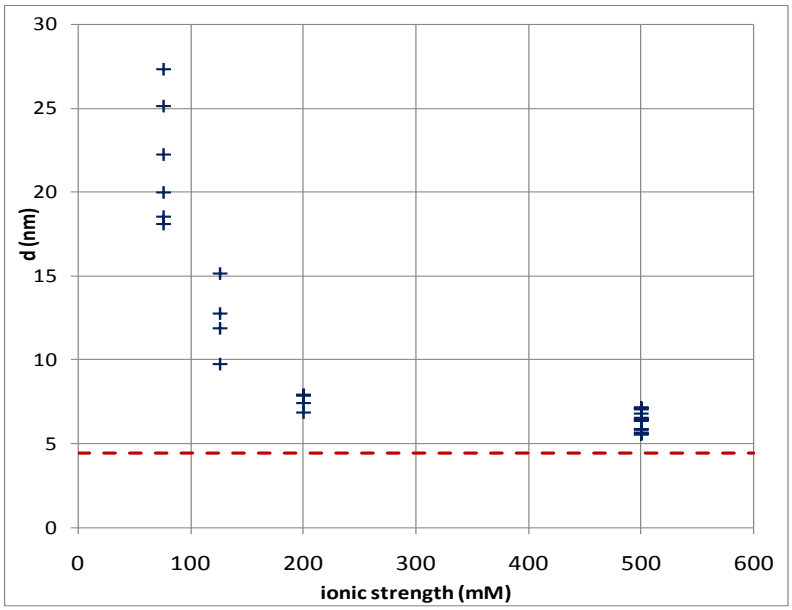

Figure III.1.5. Variation of the lamellar distance, *d*, of the C16-Cer:PA 70:30 bilayers in excess aqueous media at pH = 9.0 obtained by SAXD with the ionic strength of the aqueous medium. Each point represents an independent measurement of an independently prepared sample. The dashed line at 4.46 nm indicates the value of *d* for the ceramide in the absence of PA.

In Figure III.1.5 the experimental data should be accompanied by the prediction of the model presented in the Introduction that relates the thickness of the interbilayer aqueous layer to the properties of the medium and of the bilayer, equations 9 to 11. Until now we have not been able to calculate this line because of the scarcity of available parameters. In Figure III.1.6 we present the calculation for the forces involved in the bilayer-bilayer interaction for I = 125 mM, pH = 9.0 and a composition C16-Cer:PA 70:30. The undulations were not considered because these structures are relatively rigid as the WAXD demonstrates. The calculated Debye screening length, 8.68 Å, is quite short compared with the distance between interfaces. In fact we are dealing with a delicate play between very weak attraction and repulsion. The hydration, calculated with correlation length, λ_{hyd} = 1.93 Å and $P_{hyd,0} = 1.60\times10^{8}$ N/m^2, is only relevant at very short distances as expected from its origin. The attraction, resulting only from the London-van der Waals forces is dependent of the Hamaker constant, $H = 1.4\times10^{-21}$ J and the thickness of the bilayer including the headgroups, d_B = 4.21 nm.

If we consider that the lipid thickness is 4.2 nm and that for I = 125 mM d = 12.5 nm, the thickness of the water layer is 8.3 nm. Given the approximations, the value at which the calculated attraction and repulsion forces cancel, 9.23 nm, cannot be considered a too bad

approximation, Figure III.1.6. However, the same parameters are not able to give a so reasonable approximation to the experimental values at other ionic strengths; namely, they do not reproduce the water thickness in the absence of PA. We are still in a first formulation of this tentative of fit.

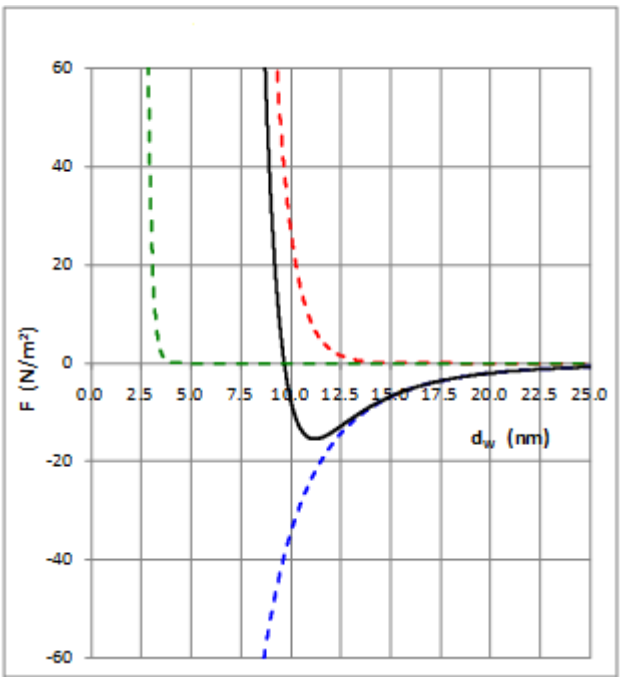

Figure III.1.6. Calculated forces for the interaction of 70:30 mixtures of C16-Cer with PA for I = 125 mM and pH = 9.0. The dashed curves represent the individual forces: hydration repulsion (green), electrostatic repulsion (red) and London-van der Waals attraction (blue). The solid line is the sum of these three components and crosses the zero force corresponding to the minimum of energy at 9.23 nm.

(iv) C16-Cer : PA structure as a function of PA molar fraction for I = 125 mM. Despite the relatively small number of experimental points, it is evident from Figure III.1.7 that the addition of a fatty acid for a given *I* increases the bilayer spacing. Above 70 mol% PA all samples display the signal of the free fatty acid and are not included in this plot. As before, a theoretical fit to those experimental points should be possible to calculate but it has not been yet done.

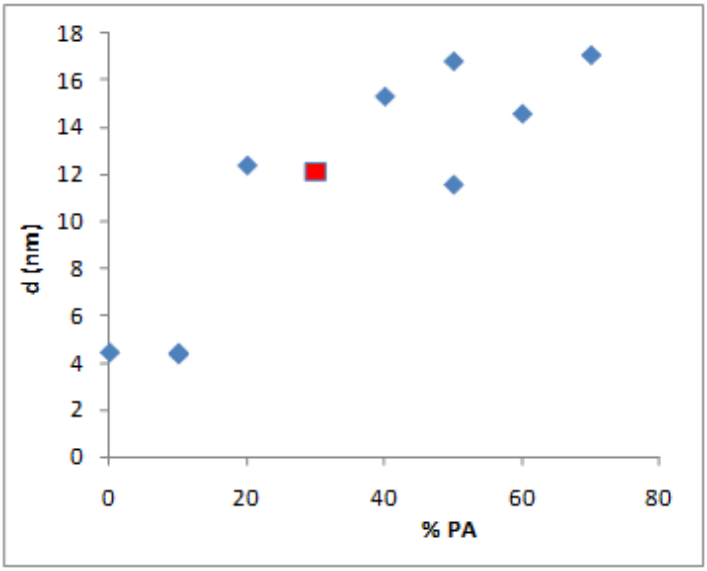

Figure III.1.7. Plot of the repeat distance determined for C16-Cer bilayers containing different amounts of PA for *I* = 125 mM and pH = 9.0. The red marker indicates the average of the measurements of four independent samples with 30 mol% PA, the others being obtained from a single sample.

Just as a curiosity we present Figure III.1.8 of the X-ray of a mixture 1:1 of C16-Cer and PA. While the WAXD shows that there is molecular arrangement of the chains not differing from what is observed for the 7:3 composition, the SAXD is very broad clearly indicating that the stacking of the lamellae is nearly inexistent and irregular as would be expected for these strongly negatively charged bilayers in the absence of enough ionic screening.

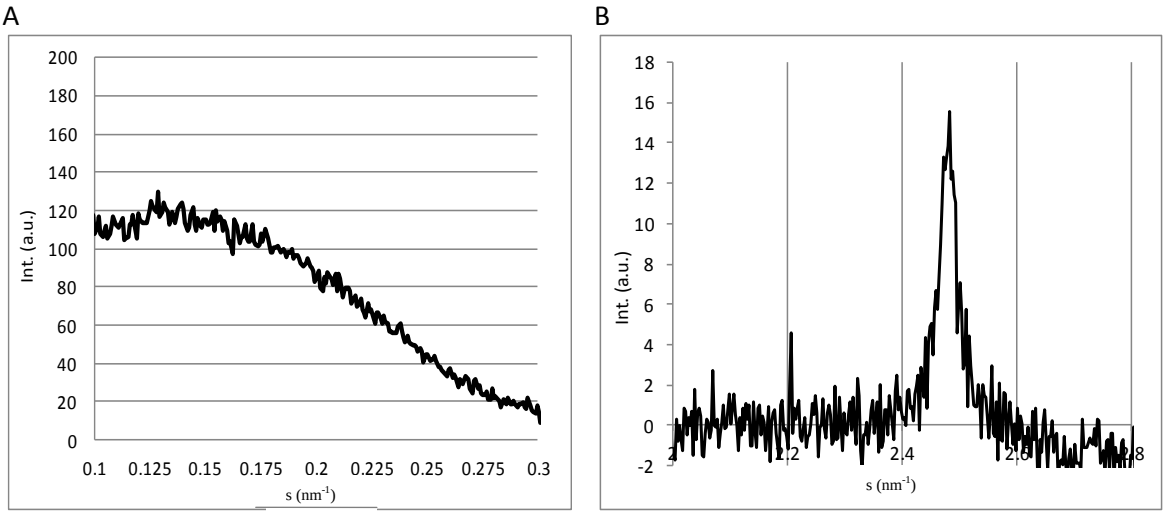

Figure III.1.8. SAXD A) and WAXD B) signals of the C16-Cer:PA 1:1 bilayers at 20 ºC for the *I* of the buffer medium of 76 mM and pH = 9.

III.2.Thermotropic behavior of Cer16:PA at pH 9

Results and discussion

(i) C16-Cer meso and molecular structure in excess water. In Figure III.2.1 the small and wide-angle diffractograms of pure ceramide as a function of temperature and *I* are presented.

In the same Figure panels B) and C) showing the WAXD structure where the two families of diffraction peaks as presented in Table III.1.1 for 20 ºC and attributed to phases α and β are observable. Upon heating, the signal of phase α remains quite constant while the peaks attributed to phase β drift to lower reciprocal distances and begin to merge with the remaining peaks at ca. 60 ºC, Figure III.2.1C. Since the encounter of the two diffraction families result in a concomitant increase in the signal strength of the phase α, it seems that a conversion between the two phases takes place above this temperature. In the small-angle region there is not a clear distinction between α and β phases, but the disappearance of the phase β results in a small change in the trend of *s* with temperature so small that is hardly quantifiable with our instrumental resolution. However, whenever the phase β is present, an equally thin but stronger SAXD signal is obtained and a significant decrease in intensity is observed above 60 ºC. So, it seems that the phase β has a large influence in the number of stacked bilayers constituting an aggregate, but the coexistence of the two phases does not perturb the regularity of distances that would result into a peak with larger FWHM.

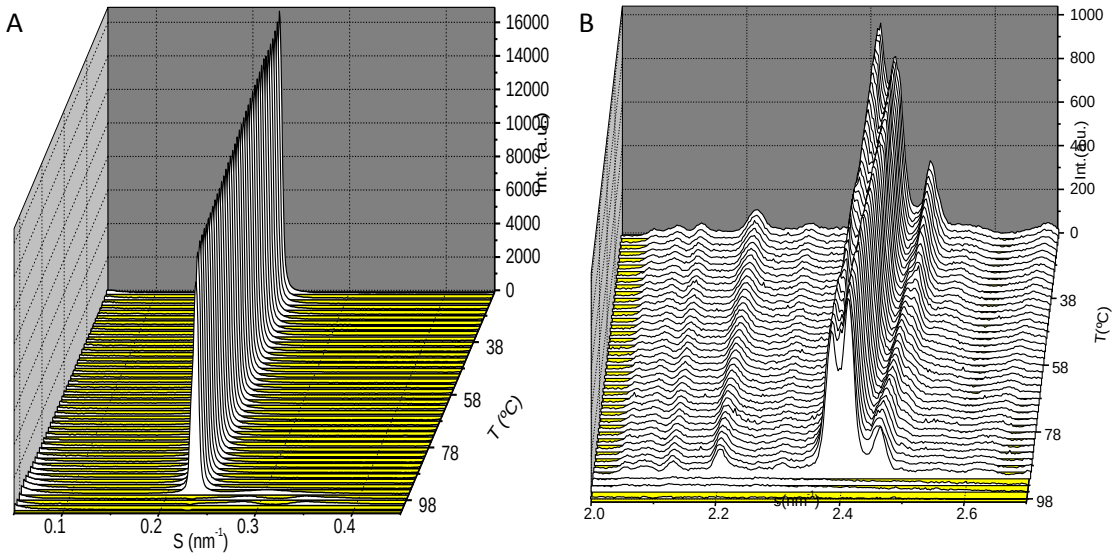

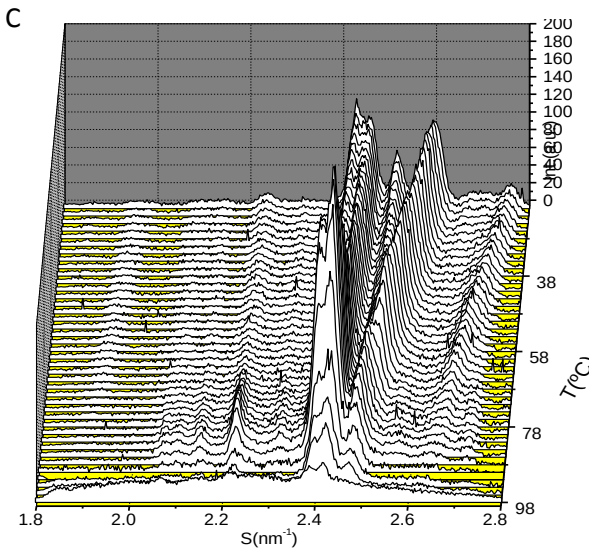

Figure III.2.1. SAXD and WAXD measurements as a function of temperature from pure C16-Cer.

The relative intensity of the signal from the two phases is not the same in all samples, the phase α being always present but the β practically absent in some cases, Figure III.2.1.B). In previous DSC determinations[52]we found that some samples had an exothermic transition with onset at 60 ºC what makes us think that we were observing the transformation of phase β in α with release of energy, and, if this is the case, the phase β is metastable at less than 60 ºC. Due to the rigidity of crystalline ceramide resulting from the strong H-bonding between headgroups and small dipole repulsion, even when very slowly cooled, the ceramide remains sometimes partially trapped in the β arrangement. Metastable states that are maintained without change at room temperature have been frequently reported for systems involving ceramides[29,97,98]. In the course of our study we could not correlate a particular behavior of the sample in which concerns the relative intensity of the signals originating from the two phases α and β with a given method of preparation, *I* or pH.

(ii) Coexistence of thin and thick phase. Perfectly uniform mixtures of C16-Cer with PA are not always obtained whatever the method used for sample preparation. Often, after centrifugation, non-uniform samples have a less dense optically opaque region essentially constituted by ceramide underlied by a gel-like region where C16-Cer is mixed with PA, but in many cases large regions of visually undistinguishable mixed phases are observed. Such samples are not considered in the study presented above, but it is relevant to state that their SAXD exhibits simultaneously characteristics of the well packed ceramide bilayers and of the water-spaced charged bilayers. For example in Figure III.2.2, which is one of the several

cases where we detected such mixture, the sample has a diffraction at 12.5 nm from the PA rich phase and a slightly larger 4.55 nm C16-Cer (the usual distance being 4.48 nm) probably due to some small contamination of PA.

Also the spacing between bilayers is larger then what is expected for similar mixtures because, due to the depletion of ceramide, the layers are richer in PA. In these samples the WAXS is also a mix of the characteristics of both phases. It is remarkable, as previously stated, that the presence of mixed phases is not related with a particular method of preparation. For example, the sample that originated Figure III.2.2 was obtained with flash-freeze that in principle should ensure a better mixing, but similar results could be found in samples created with all methods.

Even if without statistical accuracy we would venture that about 1/3 of the samples of C16-Cer with palmitic acid in the molar proportion of 7:3 hydrated with pH = 9.0 buffer at 98 ºC present coexistence of the two phases in their SAXD and WAXS pattern. However, the quality of the samples has not a clear relation with the method of preparation. The same kind of result, we can call it success, is to be expected from hydration of the precipitate obtained from anhydrous or hydrated organic solvents, and from molecularly random dispersions of freeze dried powder.

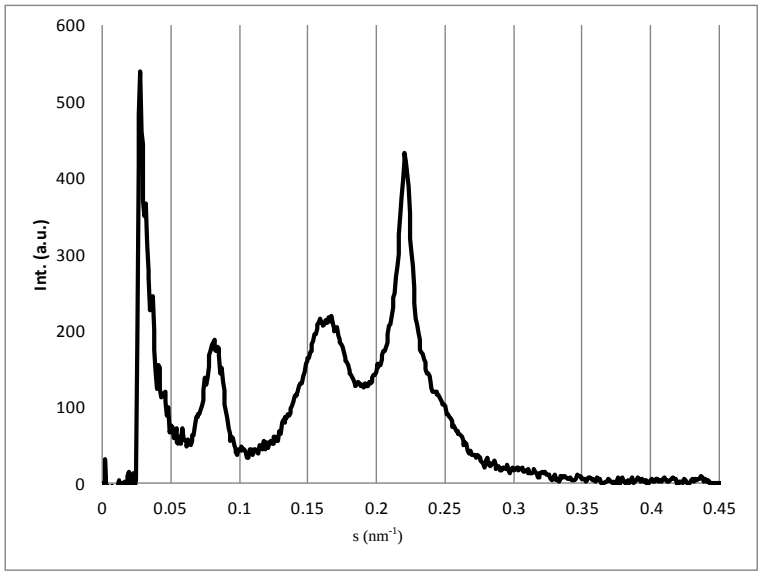

Figure III.2.2. SAXD measurement of a mixture of C16-Cer : PA in a proportion of 7:3.

It is understandable that if pure ceramide aggregates are formed at the hydration step they will not incorporate at a later time other components whether fatty acids or cholesterol as we have previously observed. So, it seems that it is the hydration speed and temperature at which the

initial hydration takes place, that are quite difficult to consistently reproduce, is the key step for the final organization of the mixture.

The data presented in the following sub-sections must be taken with some caution. They are, obtained for mixtures of C16-Cer: palmitic acid in several relative molar fractions for several ionic strengths and as a function of temperature. The systems involving ceramides, as already mentioned and detailed in the sub-section (ii) Coexistence of thin and thick phase, are rigid even when PA is added. The consequence is that they are easily trapped in unstable states even after annealing. From our experience, the only way to circumvent this difficulty is by preparing and measuring a large number of samples eliminating those that do not show a common behavior. This is reflected for example in the number of data points displayed in Figure III.1.5. Next data are, in most cases, single experiments in regions of composition for which we do not have clues for the phases to be "expected". This means that the main objective will be to analyze the thermotropic evolution of the particular samples under study with any compromise about the state of thermodynamic equilibrium of the starting mixtures.

(iii) C16-Cer:palmitic acid (8:2) structure as a function of I. For the samples with 20% palmitic acid the structural arrangements, as observed in the SAXD patterns, is ionic strength dependent, Figure III.2.3. In panel A, for 125 mM, at low temperatures there are two peaks, one very broad from a lamellar expanded phase at s = 0.204nm^{-1} with a correctly positioned second order peak on top of which a better defined peak at s = 0.221 nm^{-1} from which the second order is probably too small to be visible. The broad diffraction disappears at 66°C with a concomitant increase of the sharper s = 0.222 nm^{-1} peak that is the only detectable phase until 88 ºC. Between 92 and 98 °C a sharp and defined diffraction appears at s_1 =0.191 nm^{-1} and another broader peaks, in a ratio of √3 and √4 corresponding to one inverted hexagonal (H_{II}) phase. Between the transitions from lamellar to hexagonal we can distinguish, in only two frames, an Im*3*m inverted cubic phase, corresponding to the (200) (211) and (220) planes, with spaces in a ratio of √4, √6 and √8 respectively (s_{200} = 0.095 nm^{-1}, s_{211} = 0.132 nm^{-1}, s_{220} = 0.164 nm^{-1}).

Samples with ionic strength of 76mM, Figure III.2.3.B, present more defined and clear diffractions. During the thermal evolution, the first order peak, until 86 °C, typical from one lamellar phase at s = 0.222 nm^{-1} (4.50 nm) appears. At 88 °C, the three characteristic

reflections from the hexagonal inverted phase with estimated positions of s_1= 0.217nm^{-1} (4.60 nm) and another two peaks in ratios of √3: √4.

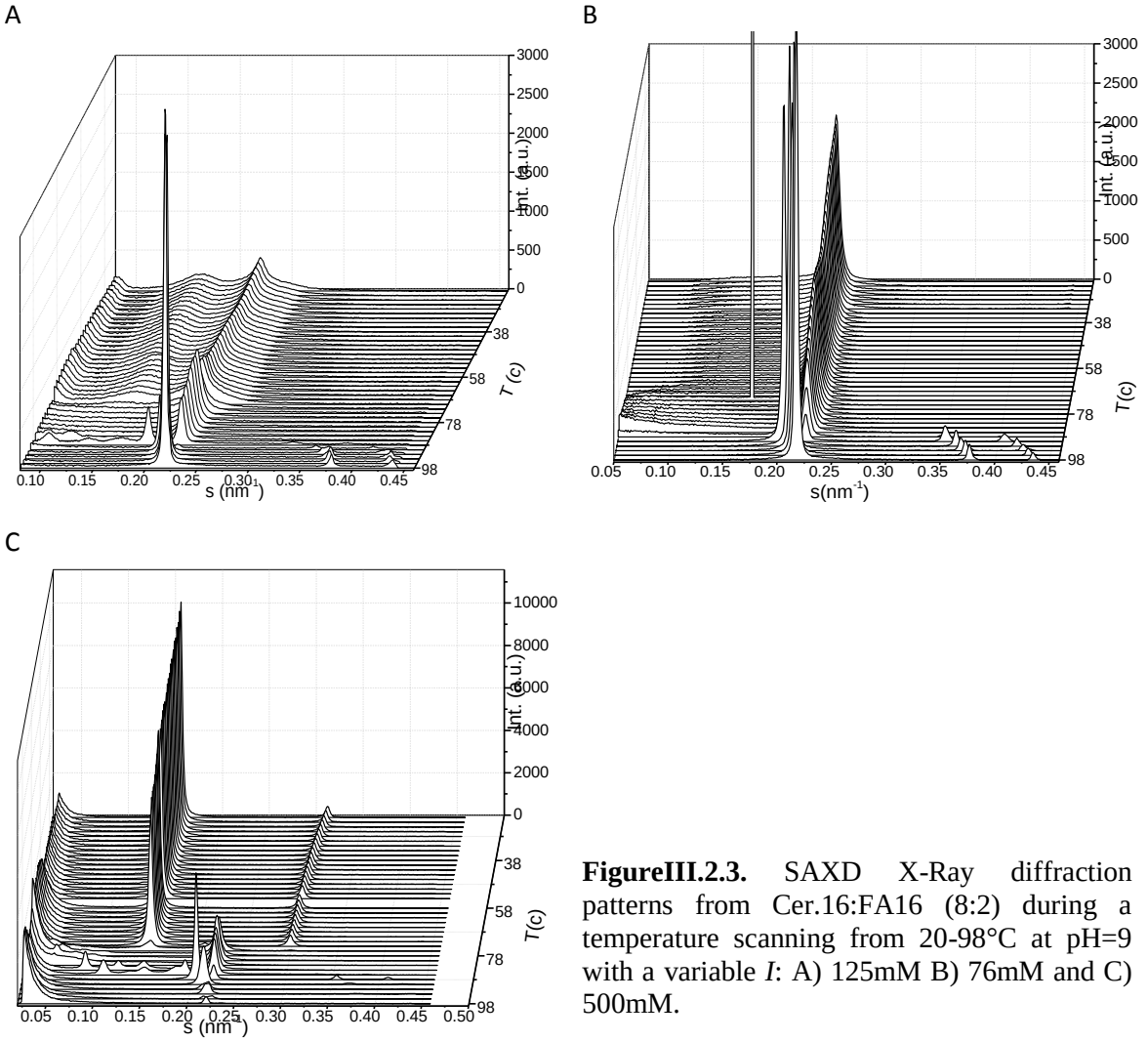

FigureIII.2.3. SAXD X-Ray diffraction patterns from Cer.16:FA16 (8:2) during a temperature scanning from 20-98°C at pH=9 with a variable *I*: A) 125mM B) 76mM and C) 500mM.

A typical diffraction of lamellar phase is also present in samples with higher salt concentration (500mM), until 76 °C, w a lamellar repetitive distance, *s*=0.156 nm^{-1} (6.41 nm) with a well defined second order peak. A detailed analysis of the diffraction patterns taken at 84 and 86°C shows the metastability of the reflections with a typical sequence of an Im3m inverted cubic phase. Simultaneous to this Im3m cubic phase we also detected another less defined cubic pattern, although their peaks definition don't allows us identify their positions with precision.

This thermotropic behavior is characteristic of dyacil phospholipids in excess water, namely phosphhatidylethanolamines[12,99], at some characteristics temperatures above the chain-

melting transition temperature, as we said in the introduction. As we can see the increasing in *I* lead to the formation of inverted cubic phases, this is can be explained by the energetic contributions already explained in the introduction chapter.

Gruner [100] also justify this behavior, as we said before, in based on geometric factors: the magnitude of the monolayer spontaneous radius of curvature of the lipid-water interface, R_0, has been postulated as a major factor in determining phase structures. Lipid systems with intermediate R_0 values between that of L_α phase (large R_0) and H_{II} phase (small R_0) are likely to form inverted hexagonal and cubic phases[101]. This explanation can also be invoked to explain our results. The rigidity of ceramides also plays against the formation of cubic and hexagonal phases involving a complex molecular rearrangement of the original lamellar structures. The speed of our T scan (1 ºC/min) is probably too fast for these stiff systems. Transitions between the lamellar and inverted cubic phases or inverted hexagonal phases are of particular interest because of the change in geometry. Siegel[101] proposed the transformation between the L_α phase and both the Q_{II} and H_{II} phases that take place via micellar intermediates[15]. These intermediates are the precursors of the H_{II} phases and of bicontinuous cubic phases[101.] The cubic phase most directly related to the interlamellar attachment is Im*3*m which has an octahedral arrangement of rods. The same author gave another explanation for these transitions based on the energetically favorable pathway from the inverted micellar intermediates[101].

(iv) C16-Cer:palmitic acid (7:3) structure as a function of I. Figure III.2.4 shows a sequence of SAXD diffraction patterns from a binary system with 125 mM of C16-Cer:palmitic acid in a proportion of 7:3. Since 20°C, we can observe one diffraction pattern with first, second and third order reflections for a lamellar expanded structure with a higher repetitive distance of d=12.151 nm (s = 0.0823 nm^{-1}), this diffraction originates at 74°C a typical C16-Cer lamellar interdigitated structure with a position of s = 0.222 nm^{-1} (4.51 nm). This structure coexists with the second and third order diffraction for hexagonal phase that appears between 74 and 98°C. In a range from 72-98°C another combination of diffractions coexisting with the previous ones, describes two different cubic phases patterns; a well-defined and clear Im*3*m and another with less defined spacings but identified as a micellar cubic phase P$4_3$32, relate with the (111) (210) and (211) planes (s_{200} = 0.066 nm^{-1}, s_{210} = 0.089 nm^{-1}, s_{211} = 0.112 nm^{-1}).

In Figure III.2.4.B), 76 mM, the lamellar expanded structure presents, since 20 to 72 °C a broad and less intense diffraction at s = 0.111 nm^{-1} following by respective second and third orders. This diffraction originates between 68 and 84°C a lamellar interdigitated structure at s = 0.222 nm^{-1}(4.50 nm) that coincide with peak positions of pure ceramide; above 84 to 98 °C begins to appear a typical pattern of an inverted hexagonal phase.

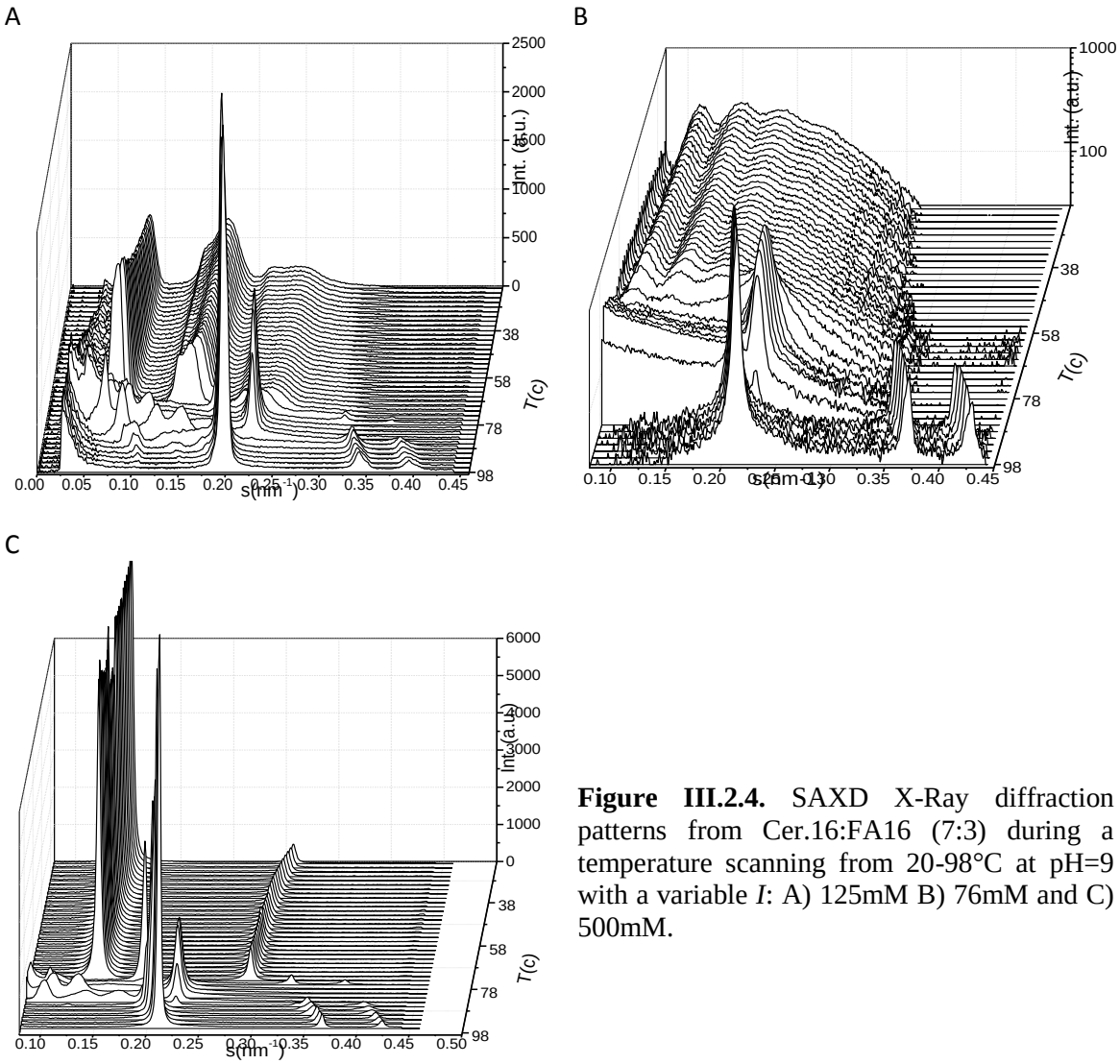

Figure III.2.4. SAXD X-Ray diffraction patterns from Cer.16:FA16 (7:3) during a temperature scanning from 20-98°C at pH=9 with a variable *I*: A) 125mM B) 76mM and C) 500mM.

Figure III.2.4.C) present clean and defined diffractions with high salt concentrations (500 mM). One lamellar structure at s = 0.1458 nm^{-1} (6.86 nm) and the respective second order is observed between 20 and 74 °C. After 74 to 98 °C a typical diffraction of an inverted hexagonal phase coexists with the two meta-stables cubic phases identified above as Im3m and $P4_332$.

When the concentration of palmitic acid is increased, a new micellar cubic phase, $P4_332$, raised. This behavior, as explained above, is related to the geometrical structure changes in ceramide C16 and shared by other lipids. Siegel[101] proposed that this transformation takes place via micellar intermediates[15] which are the precursors of the H_{II} phase and of bicontinuous cubic phases[101].

(v) C16-Cer:palmitic acid (5:5) structure as a function of I. In samples with equivalent content of palmitic acid and ceramide C16, similar SAXD patterns are acquired when compared to the earlier measurements with the same salt concentration.

Sample with 125mM of ionic strength, Figure III.2.5.A), presents a lamellar expanded phase at s = 0.086 nm^{-1} (11.63 nm). This diffraction leads to a well-defined H_{II} phase between 72 and 98 °C at s = 0.194nm^{-1} (5.15 nm) follow by two diffractions orders with ratios of √3: √4.

During 72 and 86°C one unstable cubic phase, can be observed, with diffractions representative from Im3m cubic phase that relate with the (200) (211) and (220) planes (s_{200} = 0.060 nm^{-1}, s_{211} = 0.085 nm^{-1}, s_{220} = 0.105 nm^{-1}).

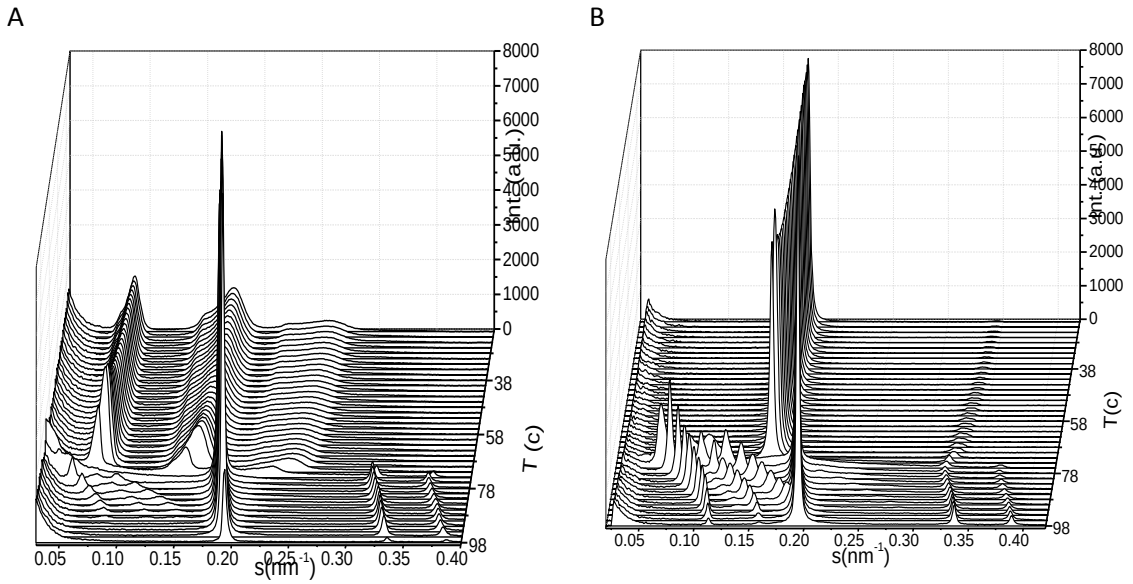

Figure III.2.5. SAXD X-Ray diffraction patterns from Cer.16:FA16 (5:5) during a temperature scanning from 20-98°C at pH = 9 with a variable *I*: A)125mM B) 500 mM.

The increasing in salt concentration (500 mM) leads to cleaner and thinner peaks. During the thermal evolution, at low temperatures, SAXD pattern is defined by a lamellar diffraction, followed by a sequence of metastable reflections since 74-98°C representatives of Im3m

inverted cubic phase in simultaneous with another inverted cubic phase, Pn3m, indexed to the (111), (200) and (211) planes (s_{110} = 0.077 nm^{-1}, s_{200} = 0.114 nm^{-1}, s_{211} = 0.134 nm^{-1}).

This mixture presents the typical behavior observed in lipids in excess water. As we explain above the phase transitions from lamellar to non-lamellar phases involved activated membrane process, the membrane fusion or the tendency to spontaneous curvature may affect the activity[101].

III.3. Preliminary studies with C10-Ceramide

(i) C10-Cer meso and molecular structure in excess water: The dispersions of C10-Cer in aqueous media do not differ in its visual aspect from those of C16-Cer. The SAXD also presents a single sharp peak, Figure III.3.1.A), at 0.259 nm^{-1} (3.86 nm), at 20 ºC, 0.619 nm less than those of C16-Cer accounting for the smaller chain length. Since the sphingosine side is of fixed C16 length we would expect the tails to be interdigitated at the center of the bilayer resulting in a decrease of thickness roughly identical to 6 C-C bonds as observed. The WAXS, that is much simpler than that of C16-Cer, at 20 ºC shows two well resolved diffractions the largest one at 2.42 nm^{-1} and a smaller peak at 2.52 nm^{-1}, figure III.3.1,corresponding to a hexagonal chain arrangement with $a = b$ = 5.0 Å. The higher symmetry is probably a consequence of the interdigitation of the tails.

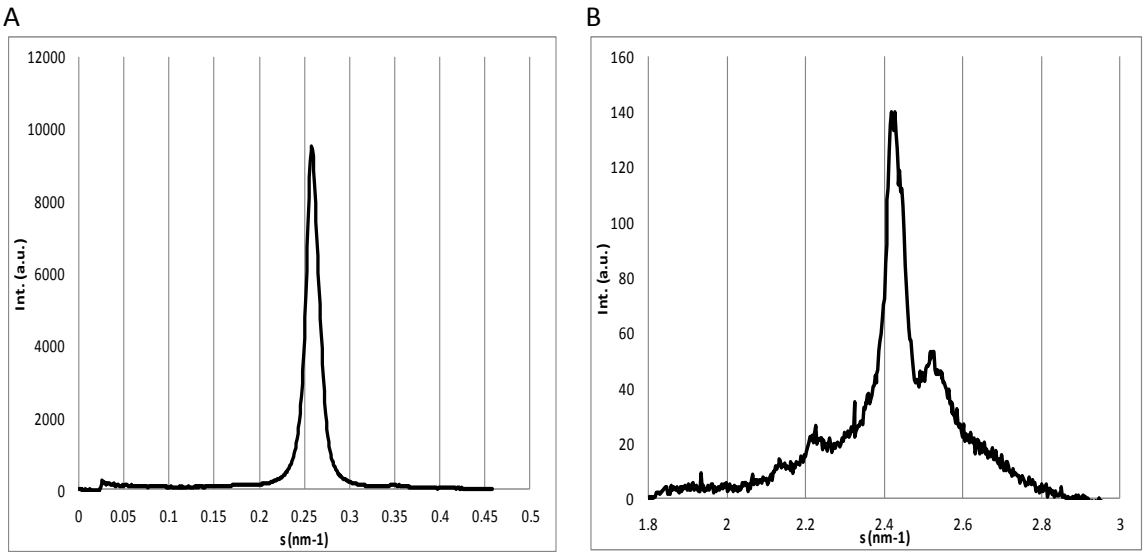

Figure III.3.1.SAXD A) and WAXD B) signals of the C10-Cer bilayers at 20 ºC for the *I* of the buffer medium of 125 mM and pH = 9.

III.4. General Conclusion

In this work we have until now shown that non-hydroxyceramides do not form the thick phases observed in the SC in particular that the thick phases observed by several authors are artifacts resulting from sample preparation[102,103], as shown in Figure III.2.2. Ceramides with fatty acids form regular bilayers and ceramides alone in excess water also form bilayers. The small repeat distance observed is due to the reduced hydration of these layers, the reason for which is not totally understood and we sustain that it is related to the low polarity of ceramide interface as compared with that of phosphocholines. The thick phase observed in *in vivo* SC104104 is probably related with properties of hydroxyl ceramides that constitute 70 % of the total ceramides present in the SC. Supporting this proposal is the relatively recent finding that the repeat distance of the so called thick phase is not necessarily of 13 nm [104], as it was for many years believed[105,106]. Layers with thickness multiple of 4.6 nm are abundant in the SC lipid matrix, while being logic, this possibility leaves the question of where the FA rise in such structure unanswered[107].

Hydrated ceramides are capable, of displaying a wide range of polymorphism, depending on the molecular structure and environmental conditions. The thermotropism of mixtures of C16-Cer with several fractions of palmitic acid and ionic strength, in excess water, resulted in a

general overview of the possible phases and phase transformations that may occur in this system.

When adding 20, 30 or 50 % of fatty acid to the ceramide with a minimum of *I* (76 mM) we started with a lamellar structure that will originate, after the chain melting temperature, an inverted hexagonal phase. As with other thermotropic transitions, the thermodynamics of this transition is generally determined by the energetic contributions.

Increasing the ionic strength, binary system becomes more complex, during the thermal expansion one or more metastable cubic phase raise between the lamellar and the inverted hexagonal phases, due to the geometrical shape constrains. Ceramides in mixture with Palmitic acid had the typical behavior from diacyl phospholipids, where the lamellar structure of the long chain is the lamellar bilayer. Our system also has the tendency to form non-lamellar phases, which are involved in activated membrane process. Explained by the disruption of the normal lamellar topology or the tendency to spontaneous curvature of the membrane.

III.5. Further work

The work based on ceramides fatty acid interaction presented above is still preliminary. There are two aspects that should be further developed before publication. The first is to model the bilayer spacing as a function of *I*, and the second to obtain the electronic density profiles from SAXD measurements in the case of low *I*.

The distance between layers results from the play between the attraction and repulsion forces between bilayers[14]. The only component of the attraction forces is the van der Waals-London force described by Verwey and Overbeek in 1948[44]. Repulsion involves components of the "hydration forces", undulation forces and electrostatic repulsions[108,109]. With the present knowledge is not easy to calculate many of these components, the van der Waals interaction is parameterized by the Hamaker constant never determined for ceramides. The physical nature of the "hydration forces" is still a question of discussion and there is no way to be calculated only based on the chemical characteristics of the interface. Bilayer undulations will not affect the quite rigid bilayers of ceramide and probably are irrelevant for the calculation. The electrostatic repulsions are the only parcel whose calculation is supported by a relatively well establish theory[44,110]. At the moment what we know is that the theory cannot model the more

common DOPC bilayer spacing but we are confident that it will give some insight in the case of ceramides.

The determination of the electronic profiles of the bilayers[111, 112], will allow to further confirm that X-ray signal originates in bilayers and should be done for the data at low *I* where the number of the SAX peaks observed, 4 or 5 orders, allows this calculation. This is important because there is a research group that interprets similar results as supporting the existence of a thick phase similar to those presumed to exist in the SC lipid matrix.

IV. Experimental methods

IV.1. Materials

(i) Origin of reagents. The phospholipids 1,2-dioleoyl-*sn*-glycero-3-phosphocholine (DOPC), 1-palmitoyl-2-oleoyl-*sn*-glycero-3-phosphocholine (POPC), 1,2-dilauroyl-*sn*-glycero-3-phosphocholine (DLPC), 1,2-dimyristoyl-*sn*-glycero-3-phosphocholine (DMPC), were obtained from Avanti Polar Lipids. The synthetic ceramide (2S, 3R, 4E)-2-hexadecanoylaminooctadec-4-ene-1,3-diol (N-palmitoyl-D-*erythro*-sphingosine) was also obtained from Avanti Polar Lipids (Birmingham, AL, USA).

Chloroform, Benzene and methanol were from Lab-Scan, HPLC grade, and NaCl Riedel de Haën, p.a. grade. Sodium azide, succinic and palmitic acids were from Panreac (Barcelona, Spain). Sodium chloride, sodium hydroxide and disodium salt of ethylenediaminetetraacetic acid (EDTA) were from Merck (Darmstadt, Germany), and boric acid from Riedel-de-Haën, (Seelze, Germany). All chemicals were used without further purification except for benzene and methanol that were dried with anhydrous magnesium sulfate (Riedel-de-Haën) distilled and kept in a dessicator over phosphorous pentoxide before use.

Ethyl ether (Lab-Scan, HPLC grade) was freed from peroxides by passing through a column containing aluminum oxide as recommended by Dasler and Bauer [113] and regularly checked for peroxide buildup using the potassium iodide test.

Water for buffer preparation was double distilled and further purified with an Elgastat UHQ-PS system (Marlow, U.K.). All the water for lipid hydration was 0.05 mM in EDTA.

Buffers were borate for pH = 9.0 and succinic acid for pH = 4.0. Care was taken that the strength of the buffer was sufficient to handle the concentrations of added PA. The desired amount of NaCl was supplemented to the buffer to obtain a final *I* of 76 (no NaCl), 125, 200 and 500 mM, being the total Na^+ concentration 50, 120, 170 and 430 mM respectively.

(ii) Lipid purification. All phospholipids, even when kept under Argon at –20 ºC, have a residual amount of lysed lipid that may not be detected with the usual TLC test, but is revealed by the appearance of foam when hydrated. To clean the phospholipids (for ceramides it is no necessary) we prepared MLV by the standard film method and submitted the suspension to several cycles consisting of freeze-thaw, followed by centrifugation and resuspension of the pellet in pure water, that were repeated until no more foam is observed. Excess water from the last pellet was removed by vacuum (10^{-2} mmHg, 2h at room

temperature). The dry precipitate dissolved in benzene was evaporated to remove the remaining water by azeotrope distillation. Lastly, the lipid was freeze-dried from benzene, the powder kept in an inert atmosphere at –20 ºC and used within one month. All manipulations of unsaturated lipids in this and subsequent preparations were done under nitrogen or argon.

IV.2. Preparation of lipid aggregation in aqueous media

(i) Preparation of MLV. Since one of our concerns is the uniformity of hydration of the lipid forming the multilayered structures, we tested several variants of the conventional MLV preparation technique[114] for phosphocholines. The starting state of the lipid before hydration was either a "film" obtained from solvent ($CHCl_3$) removal in a rotary evaporator or the powder formed by freeze-drying from benzene. In both cases two hydration protocols were tested that are here named "fast" and "slow" hydration. In the fast hydration method the aqueous media is directly added to the lipid at a temperature above the lipid main phase transition without a previous exposure to a humid atmosphere. The slow hydration was identical to the fast except that the addition of aqueous phase was done after keeping the lipid, powder or film, for 24h in 98% humidity, also above the main phase transition temperature of the lipid. In an attempt to reorganize the lamellar arrangement some samples were subjected to freeze-thaw cycles followed by slow annealing. Due to the possible accidental inconsistency in the preparation, at least two independent samples were made with each method. As an alternative to hydration with water, we also used 100 and 500 mM NaCl.

When we wanted to maintain the samples at the same temperature from hydration until measurement, the freeze-dried lipid powder was transferred to a vial and the aqueous media added at the required temperature. The temperature was maintained along all manipulations, including overnight hydration, centrifugation, transfer to the capillary and subsequent centrifugation and closing. The sample was stabilized for 2 days at the same temperature and directly transferred to the pre-heated sample-holder.

In the case of ceramides, the common method of hydration of the lipid film obtained by organic solvent evaporation is not adequate for lipid mixtures because it frequently leads to lipid separation in the solvent evaporation step[115]. We previously observed that this is particularly true when one of the components is a ceramide, the individual excluded component being easily detected by DSC and/or X-ray diffraction of the aqueous suspension.

One of the methods to avoid lipid separation is to sublimate the organic solvent containing the lipid mixture, leaving the lipids randomly organized in the solid state before hydration[115]. The method is well established: the lipids stock solutions in dry benzene/methanol, 7:3 (v:v) are mixed in adequate amounts and allowed to equilibrate for about 30 minutes with occasional vortexing and the solution frozen at –20 ºC for at least 2 hours and subsequently freeze-dried. In the case of poorly soluble lipids that tend to precipitate in the freezing step, as is the case of ceramides, we quench in liquid N_2 the solution contained in thin-wall glass tubes obtaining a vitreous solid with no sign of lipid precipitation that is transferred without melting to the freeze-dryer. For hydration step, 0.3 ml of buffer at 98 ºC was rapidly added to the powder obtained from freeze-drying and the dispersion hydrated at 98 ºC for 30 min with occasional shaking, centrifuged at 30 kG for 10 min.

(ii) Preparation of MLV-REVs. Multilayered REV vesicles were prepared using the method developed by Pidgeon et al., that is based on the reverse phase evaporation technique for formation of large unilamellar vesicles, in which the ratio between the mass of lipid and water is increased by ca. 10×[26,27]. For X-ray samples 100 mg of lipid were dissolved in 2ml of diethyl ether, into which 60 µl of aqueous media was rapidly injected. The sample was sonicated under argon for 2 min at 25 ºC and the ether evaporated in a rotary evaporator at 37ºC and 700 mmHg until formation of a semi-solid gel. The gel was vigorously agitated in a vortex to induce emulsion inversion, easily noticed by the change of the fluidity of the suspension, and the remaining organic solvent removed in the rotary evaporator at 37ºC and 450 mm Hg. To eliminate small lipid aggregates that may be present, the preparations were washed twice with the aqueous media and centrifuged at 10 000G for 10min. The residual ether was removed by overnight dialysis against the aqueous media saturated with nitrogen.

(iii) Preparation of extrusion LUV (LUVET). Large unilamellar vesicles, LUV, of DOPC, DMPC, DLPC and POPC were prepared by repetitive extrusion of a MLV suspension in water (1.25, 2.5 or 5 mM in lipid) with high N_2 pressure through 100 nm pore Nuclepore polycarbonate filters (Corning, Acton, MA, USA) at room temperature according to a well known methodology[24,25]. The final suspension was centrifuged for 10 min at 1 kG to free the solution of the more dense particles.

(iv) Samples for DLS.

Samples were prepared as we explain above (preparation of LUV) and transferred for 1 cm silica cuvettes with care to avoid the formation of bubbles. After the equipment programming with decided temperature and trend we can start the measurement.

The LUVET experiments gave clean correlation functions and a single peak with an average polydispersity index of ca. 0.075. For lipid concentrations at and below 2.5 mM identical results are obtained, and we opted to make all measurements with 1.25 mM samples. Identical experiments were tried with LUV of phosphocholines prepared by reverse phase evaporation[116], but were not conclusive due to the polydispersity of size.

(v) Samples for X-ray. Part of the hydrated lipid and a small volume of buffer were transferred to glass capillary tubes, 1.0 mm diameter with 0.01 mm wall (Markröhrchen, Germany). The open capillaries were centrifuged for 10 min at 1250 G, and, before being closed, left for 48 h under an argon atmosphere saturated with water to avoid possible oxidation processes before and during X-ray irradiation.

In the case of ceramides, before measurement the sample temperature was raised until 98 ºC, above the main transition temperature of the C16-Cer, and cooled at a rate of 0.4 ºC/min until the temperature we intended as starting point for the experiment. After this treatment no exothermic signals are observed in the heating DSC and the X-ray diffractograms are reversible, and, even after stored at room temperature for several weeks there is no modification in the sample X-ray profile. However, it is not certain that a single phase, the one with lower energy, is obtained.

IV.3. Methodologies

(i) Dynamic light scattering. With this equipment we determine the size by first measuring the Brownian motion of the particles in a sample, and then interpreting a size from these using established theories.

Data was acquired with a Malvern Nano ZS (Malvern Instruments, Malvern, UK) with only one detector at 173º. To simulate as close as possible the experimental thermal conditions used in the X-ray experiments the samples were heated in steps of 2.5 ºC, followed by a 2 min

equilibration and 10 measurements were averaged at each temperature during a trend from 5 to 70 ºC, except for DMPC, due to its high melting temperature, measurements only start at 25 ºC.

We questioned what should be the effect on the experimentally determined hydrodynamic radius, R_H, of a liposome that changes shape from spherical to a prolate spheroid with axial ratio $p = a/b$, where a and b are respectively the axial and equatorial semi-axes. The Perrin factor, $F = f_H / f_S = R_H / R_S$, relates the frictional coefficient of a diffusing object, f_H, to that of an equivalent sphere, f_S. For a prolate spheroid F can be calculated from p using the expression [117]:

$$F = \frac{\sqrt{P^2 - 1}}{\sqrt[3]{p l_n\left(p + \sqrt{p^2 - 1}\right)}} \tag{14}$$

The determination of R_S from the molar mass, M_w, and specific volume, $\bar{V}$, of the lipid, considering a monodisperse system, is straightforward,. $R_S = \sqrt[3]{3M_W \bar{V} / 4\pi N_A}$. In the calculation we considered the thickness of the solvent layer equal to 0.24 nm and the thickness of the bilayer as 4.6 nm.

(ii) X-Ray diffraction. Hydrated lipid systems, produce a diffraction pattern characterized by several Bragg diffractions at small angles, together with a set of reflections in the wide angle region. These diffraction data, although not permitting a precise atomic level structural characterization, provide important structural information.

Small angle X-ray diffraction data was collected at the synchrotron radiation facility beamline A2 of the Soft Condensed Matter laboratory at the storage ring DORIS III of the Deutsches Elektronen Synchrotron (DESY), using a setup previously described [118]. The wavelength of the X-ray beam is 0.15 nm and the detectors were a Mar165 and a Gabriel-type gas detector, for SAXD and WAXS respectively.

The measurements were done with the capillary in a temperature-controlled holder first slowly cooled from room temperature until 4 ºC (20 ºC in the case of ceramides) and then heated until 86 ºC (98 ºC for ceramides) at 1.0 ºC/min, maintained at 86 ºC for 4 min, to check for sample structural stability, and subsequently returned to 20 ºC. Data acquisition lasted for

20 s every 120 s (corresponding to ca. 2 ºC). The real temperature of the sample holder at the beginning of each data collection was registered together with the corresponding CCD image. For some samples the heating was stopped at selected temperatures and kept at this temperature for 60 min with measurement every 2 min.

The SAXD region was calibrated with rat tail collagen, and the marCCD output linearized with an in-house developed program (A2tool, A. Rothkirch, Hasylab, DESY). The distance to beam center of the observed diffraction rings was converted into reciprocal spacing, $s = 1/d$, where d is the distance between the diffracting planes. A second calibration with rat tail collagen after a set of experiments confirmed the stability of the instrumental setup.

The background noise profile obtained from a long data acquisition (30×20 s) of a capillary filled with water was subtracted from the experimental diffractograms. The evaluated error in s in the SAXD region considered is of 0.001 nm^{-1}.To characterize multimodal SAXD Bragg peaks we opted to fit the data to a linear combination of Lorentzian functions using the package Origin 7 (OriginLab Co., Northampton, USA). Since a single Lorentzian is known to be quite adequate to describe the single-component diffractions, the use of other more sophisticated model equations did not add further understanding to the aspects we intend to prove.

V. Reference List

(1) Brewster, R., Pincus, P.A., Safran, S.A. *Biophysical Journal* **2009**, 97, 1087-1094.

(2) Wertz, P.W. *Acta Derm Verereol*. *Supp.* **2000**, 208, 7-11.

(3) Wertz, P., Norlén, L. Forslin, B., Lindberg, M. *American Academic of Dermatology*. Eds., Marcel Dekker, New York **2004**, 85-106.

(4) Lichtenberg, D., Robson R.J., Dennis E.A. *Biochimica et Biophysica Acta- Reviews on Biomembranes* **1983**, 737, 285-304.

(5) Ulrich-Bott, B., Wiegandt, H. *The journal of Lipids Research* **1984**, 5, 1233-1245.

(6) Tanford, C. *Wiley Encyclopedia of Chemical Biology*. John Willey and Sons Inc., New York **1973**.

(7) Tanford, C.C. *J. Am. Chem. Soc.***1962**, 84 , 4240-4247.

(8) Butler, J.A.V. *Trans. Faraday Soc*.**1937**,33, 235.

(9) Evans, D.F., Wennerstrom, H. *Fundamentals of Interfacial Engineering.* VCH Publishers, New York **1994**.

(10) Stuart, M.C.A., Boekema, E. J. *Biochimica et Biophysica Acta - Biomembranes* **2007**, 1768, 2681–2689.

(11) Marsh, D. *Handbook of Lipid Bilayers* **2012**, CRC Press, Boca Raton.

(12) Seddon, J.M. *Biochim. Biophys. Acta* **1990**, 1031, 1-69.

(13) Kinnunen, P., Laggner, P. *Phospholipid phase transition* **1991**, 57, Elsevier Scient. Pub. Ireland Ltd.

(14) Helfrich, W. *Z. Naturfosch* **1973**, 28c, 693-703.

(15) Siegel, D., *Biophys. J.* **1984**, 45, 399-420.

(16) Arvidson, G., Brentel, I., Khan, A., Lindblom, G., Fontell, K. *Eur. J. Biochem.* **1985**, 152, 753-759.

(17) Feng, Y., Yu, Z., Quinn, J.P. *Chem. Phys. lipids* **2003**, 126, 141-148.

(18) Sun, R.G., Zhang, J. *Acta Chim. Sinica* **2007**, 65, 246-252.

(19) Vaz, W. *Wiley Encyclopedia of Chemical Biology*. John Willey and Sons, New York **2008**.

(20) Nagle, J.F. *Ann. Rev. Phys. Chem.* **1980**, 31, 157-195.

(21) Cevc, G., Marsh, D. *Phospholipid Bilayers. Physical Principles and Models*. John Wiley & Sons, Inc., New York **1987**.

(22) Smorodin, V., Melo, E. *J. Phys. Chem. B* **2011**, 105, 6010-6016.

(23) New, R.R.C. *Liposomes a practical approach*. Rickwood, D., Hames, B.D. New York **1989**.

(24) Szoka, F., Olson, F., Heath, T., Vail, W., Mayhew, E., Papahadjopoulos, D. *Biochimica et Biophysica Acta* **1980**, 601, 559-571.

(25) Mayer, L.D., Hope, M.J., Cullis, P.R. *Biochimica et Biophysica Acta* **1986**, 858, 161-168.

(26) Piedgeon, C., Hunt, A.H.,Dittrich, K. *Pharm. Res* **1986**, 3, 23-34.

(27) Piedgeon, C., Mcneely, S., Schmidt, T., Johnson, J. E. *Biochemistry* **1987**, 26, 17-29.

(28) Winter, R. *Biochimica et Biophysica Acta* **2002**, 1595, 160-184.

(29) Shah, J., Atienza, J. M., Duclos, R.I., Rawlings, A.V., Dong, Z. X., Shipley, G.G. *J. Lipids. Res.* **1995**, 36, 1936-1944.

(30) Lagüe, P. Zuckermann, M.J.; Roux, B. *Faraday Discuss*. **1998**, 111, 165-172.

(31) Luzzati, V.; Husson, F. *J. Cell Biology* **1962**, 12, 207.

(32) McIntosh, T.J.; Simon, S.A. *Biochemistry* **1986**, 25, 4948-4952.

(33) Evans E.; Skalak, R. *Mechanics and Thermodynamics of Biomembranes* **1980**, CRC Press Inc., Boca Raton.

(34)Valério J., Lameiro H.,.Funari S.S., Moreno M.J., Melo E.*J. Phys. Chem.B* **2012**,116,168-178.

(35) Troncoso, J., Navia, P., Romani, L., Bessieres, D., Lafitte, T. J. *Chem. Phys.* **2011**, 134, 094502-1- 094502-11.

(36) Nayar, R.; Hope, M.J.; Cullis, P.R. *Biochimica et Biophysica Acta* **1989**, 286, 200-206.

(37) Mui, B.L.S., Cullis, P.R., Evans, E.A., Madden, T.D. *Biophys. J.* **1993**, 64, 443-453.

(38) Petrache, H.I., Gouliaev, N., Tristan-Nagle, S., Zhang, R., Suter, R.M., Nagle, J.F. *Physical Review E* **1998**, 57, 7014-7024.

(39) Helfrich, W. *Journal de Physique* **1985,** 46, 1263-1268.

(40) Servuss, R. M.; Helfrich, W. *Physics of Complex and Supermolecular Fluids* **1987,** Safran, S. A., Clark, N. A., Eds.

(41) Servuss, R. M.; Helfrich, W. *Journal de Physique* **1989,** *50*, 809-827.

(42) Zhang, R. T.; TristramNagle, S.; Sun, W. J.; Headrick, R. L.; Irving, T. C.; Suter, R. M.; Nagle, J. F. *Biophys. J.* **1996,** 70, 349-357.

(43) Gordeliy, V. I., Cherezov, V., Teixeira, J. *Phys. Rev. E* **2005,** 72, 061913-1-061913-16.

(44) Verwey, E.J.W., Overbeek, J.T.G.*Theory of the Stability of Lyophobic Colloids* **1948**, Elsevier Pub. Comp., Inc.

(45) LeNeveu, D.M., Rand, R.P., Parsegian, V.A., Gingell, D. *Biophys. J.* **1977**, 18, 209.

(46) Cevc, G., Marsh, D. *Biophys. J.* **1985**, 47, 21.

(47) McIntosh, T.J., Simon, S.A. *Biochemistry* **1993**, 32, 8374.

(48) Helfrich, W., *Naturforsch. A* **1978**, 33a, 305.

(49) Evans, E.A., Parsegian, V.A. *Proc. Natl. Acad. Sci. USA* **1986**, 83, 7132.

(50) Gomez-Fernandez, J.C., Vilalain, J.*Chem. phys. Lipids* **1998**, 96, 41-52.

(51) Cevc, G. Biochim. *Biophys. Acta* **1990**, 1031, 311 – 382.

(52) Souza, S.L., Capitan, M.J., Alvarez, J., Funari, S.S., Lameiro, M.H., Melo, E. *J. Phys. Chem. B* **2009**, 113, 1367-1375.

(53) Casilla, R., Cooper, W.D., Eley. D.D. *J. Chem. Soc. faraday Trans. I* **1973**, 69, 257-262.

(54) Israelachvili, J.N. *Intermol. Surface Forces* **1985**, Academic Press, London.

(55) de Jager, M.W., Gooris, G.S., Ponec, M., Bouwstra, J.A. *J. Lipid Res.* **2005**, 46, 2649.

(56) Al-Amoudi, A., Dubochet, J., Norlen, L. *J. Invest. Dermatol* **2005**, 124, 764 – 777.

(57) Shah, J., Atienza, J.M., Duclos, R.I., Rawlings, A.V., Dong, Z. X., Shipley, G. G. *J. Lipid Res.* **1995**, 36, 1936.

(58) Moore, D.J., Rerek, M.E., Mendelsohn, R. *J. Phys. Chem. B* **1997**, 101, 8933.

(59) Chen, H.C., Mendelsohn, R., Rerek, M.E., Moore, D.J. *Biochim. Biophys. Acta* **2000**, 1468, 293.

(60) Velkova, V., Lafleur, M. *Chem. Phys. Lipids* **2002**, 117, 63.

(61) Souza, S.L., Valério, J.; J., Funari, S.S., Melo, E. *Chem. Phys. lipids* **2011**, 164, 643-653.

(62) Dahlen, B., Pascher, I. *Acta Crystallographica Section B-Structural Crystallography and Crystal Chemistry* **1972**, B 28, 2396 – 2404.

(63) Valério, J., Funari, S.S., Melo, E., unpublished work.

(64) Small, D.M. *Handbook of lipid research* **1986**, 14, Plenum Press, New York.

(65) Koynova, R., Tenchov, B. *Curr. Opin. Colloid Interface Sci* **2001**, 6, 277-286.

(66) Seddon, J.M., Templer, R.H., Warrender, N.A., Huang, Z., Cevc, G., Marsh, D. *Biochem. Biophys. Acta* **1997**, 1327, 131-147.

(67) Kitson, N., Thewalt, J., Lafleur, M., Bloom, M. *Biochemistry* **1994**, 33, 6707-6715.

(68) Abraham, W., Downing, D.T. *Biochim. Biophys. Acta* **1991**, 1068, 189-194.

(69) Clerc, S.G., Thompson, T.E. *Biophysical Journal* **1994**, 67, 475-476.

(70) Patty, P.J., Frisken, B.J. *Biophysical Journal* **2003**, 85, 996-1004.

(71) Frisken, B.J.; Asman, C.; Patty, P.J. *Langmuir* **2000**, 16, 928-933.

(72) Hunter, D.G.; Frisken, B.J. *Biophys.J.* **1998**, 74, 2996-3002.

(73) Kucerka, N., Tristram-Nagle, S., Nagle, J.F. *Journal of Membrane Biology* **2005**, 208, 193-202.

(74) Kucerka, N., Liu, Y.F., Chu, N.J., Petrache, H.I., Tristram-Nagle, S.T., Nagle,J.F. *Biophysical Journal* **2005**, 88, 2626-2637.

(75) Evans, E., Rawicz, W. *Physical Review Letters* **1990**,64, 2094-2097.

(76) Kolchens, S.; Ramaswami, V.; Birgenheier, J.; Nett, L.; Obrien, D.F. *Chemistry and Physics of Lipids* **1993**, 65, 1-10.

(77) Julicher, F., Seifert, U., Lipowsky, R. *Physical Review Letters* **1993**, 71, 452-455. Linke, G. T.; Lipowsky, R.; Gruhn, T. *Phys. Rev. E* **2005**, 71, 051602-1- 051602-7.

(78) Linke, G. T., Lipowsky, R., Gruhn, T. *Phys. Rev. E* **2005**, 71, 051602-1- 051602-7.

(79) Paz-Ramos, C., Cerdeirina, A.C., Costas, M., *J. Phys. Chem. B* **2011**, 115, 9626-9633.

(80) Needham, D., Evans, E. *Biochemistry* **1988**, 27, 8261-8269.

(81) Costigan, S. C., Booth, P. J., Templer, R. H. *Biochim. Biophys. Acta-Biomembranes* **2000,** 1468, 41-54.

(82) Tristram-Nagle, S.; Nagle, J. F. *Chem. Phys. Lipids* **2004,** 127, 3-14.

(83) Pan, J., Tristram-Nagle, S., Kucerka, N., Nagle, J. F. Biophys. J. **2008**, 94, 117-124.

(84) Safinya, C. R., Roux, D., Smith, G. S., Sinha, S. K., Dimon, P., Clark, N. A., Bellocq, A. M. *Physical Review Letters* **1986,** 57, 2718-2721.

(85) Roux, D., Safinya, C. R. *Journal de Physique* **1988,** 49, 307-318.

(86) Zhang, R. T., Sun, W. J., TristramNagle, S., Headrick, R. L., Suter, R. M., Nagle, J. F. *Physical Review Letters* **1995,** 74, 2832-2835.

(87) Laggner, P., Kriechbaum, M., Rapp, G. *Chem. Phys. Lipids* **1991,** 57, 121-145.

(88) Tenchov, B., Koynova, R., Rappolt, M.; Rapp, G. *Biochim. Biophys. Acta-Biomembranes* **1999,** 1417, 183-190.

(89) Israelachvili, J. N., Mitchell, D. J., Ninham, B. W. *Biochim. Biophys. Acta* **1977,** 470, 185-201.

(90) Nagle, J. F., Tristram-Nagle, S. *Biochim. Biophys. Acta-Rev. Biomembranes* **2000,** 1469, 159-195.

(91) Jones, J. D., Thompson, T. E. *Biochemistry* **1989,** 28, 129-134.

(92) Abreu, M. S. C., Moreno, M. J., Vaz, W. L. C. *Biophys. J.* **2004,** 87, 353-365.

(93) Huster, D., Jin, A. J., Arnold, K., Gawrisch, K. *Biophys. J.* **1997,** 73, 855-864.

(94) Mathai, J. C., Tristram-Nagle, S., Nagle, J. F., Zeidel, M. L. *Journal of General Physiology* **2008,** 131, 69-76.

(95) Evans, E., Needham, D. *J. Phys. Chem.* **1987,** 91, 4219-4228.

(96)Vogel, M., Munster, C., Fenzl, W., Salditt, T. *Physical Review Letters* **2000,** 84, 390-393.

(97) Lafleur, M. *Can. J. Chem.* **1998**, 76,1501-1511.

(98) Rerek, M.E., Chen,H.C., Markovic, B., Van Wyck, D., Garidel,P., Mendelsohn, R., Moore, D.J. *J. Phys. Chem. B* **2001**, 105, 355-9362.

(99) Mariani, P.,Luzzati, V., Delacroix, H. *J. Mol. Biol.* **1988**, 204, 165-189.

(100) Gruner, S.M. *Proc. Natl. Acad.USA* **1985**, 82, 3665-3669.

(101) Siegel, D., *Chem. Phys. Lipids* **1986**, 42, 279-301.

(102) Groen, D., Gooris, G.S., Bouwstra, J.A. *Biophys. J.* **2009**, 97, 2242 – 2249.

(103) Bouwstra, J.A., Dubbelaar, F.E.R., Gooris, G.S., Ponec, M. *Acta Derm. Venerol. (Stockh)* **2000**, 208, 23 – 30.

(104) Wartewig, S., Neubert, R.H.H. *Skin Pharmacology and Physiology* **2007**, 20, 220 – 229.

(105) Hou, S.Y.E., Mitra, A.K., White, S.H., Menon, G.K., Ghadially, R., Elias, P.M. *J. Invest. Dermatol* **1991**, 96, 215 – 223.

(106) Schreiner, V., Gooris, G.S., Pfeiffer, S., Lanzendorfer, G., Wenck, H., Diembeck, W., Proksch, E., Bouwstra, J. *J. Invest. Dermatol* **2000**, 114, 654 – 660.

(107) Bouwstra, J.A., Gooris, G. S., Vanderspek, J. A., Bras W. *J. Invest. Dermatol.***1991**, 97, 1005 – 1012.

(108) Inouye, H., Kirschner, D.A. *Biophys. J.* **1988**, 53, 235 – 245.

(109) Cowley, A.C., Fuller, N.L., Rand, R.P., Parsegian, *V.A. Biochemistry* **1978**, 17, 3163 – 3168.

(110) Ninham, B.W., Parsegian, V.A. *J. Theor. Biol.***1971**, 31, 405.

(111) Tristan-Nagle, S.; Nagle, F.J. *Chem Phys. Lipids* **2004**, 127, 3-14.

(112) Luzzati, V., Tardieu, A., Taupin, D. *Chem. Phys. Lipids* **1972**, 8, 292.

(113) Dasler, W.; Bauer, C. D. *Industrial and Engineering Chemistry-Analytical Edition* **1946,** *18*, 52-54.

(114) Bangham, A.D., Standish, M.M., Watkins, J.D. *J. Mol. Biol.* **1965,** 13, 238-251.

(115) Huang, J.Y., Buboltz, J.T., Feigenson, G.W. *Biochimica et Biophysica Acta* **1999**, 1417, 89-100.

(116) Szoka, F., Papahadjopoulos, D. *Proc. Natl. Acad. Sci. USA* **1978,** 75, 4194-4198.

(117) Burchard, W. Combined static and dynamic light scattering. *Light Scattering. Principles and development.* Brown, W. ed.*;* Clarendon Press: Oxford, **1996**.

(118) Funari, S. S., Barcelo, F., Escriba, P. V. *J. Lipid Res.* **2003,** 44, 567-575.